Contents

1.0 Introduction

The current focus of government policy and the construction industry to reduce energy usage and the carbon footprint of both new and existing constructions has led to an increased uptake in innovative new technologies to reduce the impact of the construction on climate change. As one of the largest contributors to the energy usage and therefore the emissions of structures, the reduction of electricity and gas usage for space and water heating has a high priority in order to achieve carbon reduction targets. One of the technologies which can cause a reduction in the energy requirement for space and water heating by over 75%[1] is Ground Source Heat Pumps and their application within Energy Foundations such as Energy Piles and Energy Walls.

1.1 Literature Review

Ground Source Heat Pumps (GSHPs) are an incredibly useful tool in the engineer's toolbelt for heating and cooling a structure; regulating the temperature of the building it using the large thermal mass of the soil around the structure. Over the past few decades GSHPs have been increasing in prominence throughout the world, according to The Golden Age there have been over one million units installed worldwide as of 2004 [1]. They operate by exploiting the temperature difference between the soil and the air in the structure. By installing the cooling loops at depths of greater than 10m the systems experience an almost constant temperature of around 12^{O}C in the UK (see Figure 1.1.1).

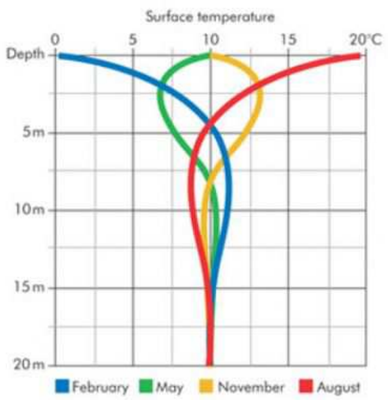

Figure 1.1.1 Annual temperature changes of soil plotted against depth. [6]

GSHPs consist of two separate pumped circuits of coolant connected by a heat exchanger; the layout of such a system can be seen in Figure 1.1.2. One of these loops is installed into the heating or cooling system of the building (secondary circuit) and the other is installed in the soil (primary circuit). By pumping the coolant, a temperature gradient is generated in the heat exchanger and can either transfer heat from the structure to the soil during the Summer cycle causing cooling of the structure and heating of the soil or heat can be transferred from the soil to the

[1] Based upon a Coefficient of Performance of between 3-6 [2]

structure in Winter effectively heating up the structure. These systems tend to have a Coefficient of Performance (CoP) greater than 3 [2]; ,meaning three times as much heat energy is transferred by the system than the electrical energy that is used to drive the heat pump

There are strong economic benefits from the operation of GSHPs as can be seen from the energy demand due to the CoP. The space heating, cooling and water heating costs are drastically reduced with the installation of an appropriate GSHP system. They come with large initial costs requiring intense geotechnical work, especially if retrofitted in an urban environment. The ability to merge the installation of GSHPs within the construction process of the foundations of a structure however massively reduces these costs. As a result energy foundations have become much more prominent over the past few decades, with a number of installations in new and existing constructions, many of which include research on the operation of the foundations including Keble College, Oxford (85kW) and the Bulgari Hotel, Knightsbridge (150kW) [3] as well as ten of twelve Crossrail stations with various Energy Foundations installed.

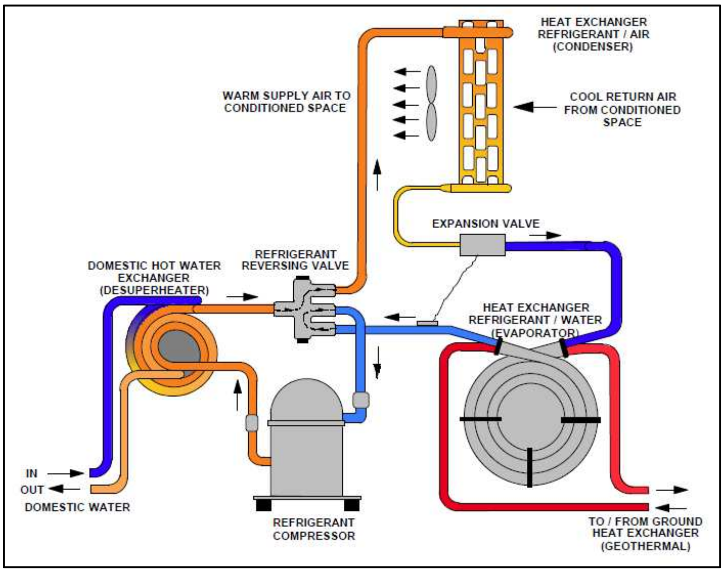

Figure 1.1.2 Components of a Ground Source Heat Pump (In an air heating, soil cooling cycle) [5]

Energy Foundations essentially incorporate the ground side coolant loop within the construction of a new foundation. These can be installed in piles, tunnels or diaphragm walls. These benefit from the strength and thermal properties of the concrete both protecting and allowing for good thermal properties. The impact on the project causes a slightly longer foundation installation by attaching the loops to the reinforcement cages however the effect is minimal.

There has been limited research upon the operational effects of heating and cooling cycles on energy walls and other thermo-active foundations. Brandl discusses in 2006 paper [4] the effects of heat exchangers built into “earth-contact concrete elements that are already used for structural reasons" and discusses the heat transfer between the concrete structure and the ground. Bourne-Webb et al's study in 2009 [5] focuses upon the "geotechnical performance of piled foundations incorporating pipe loops for ground-source heat-pump systems" due to the impact of heating and cooling cycles. However there is very little research specifically upon the effect of heating and cooling cycles upon the geotechnical aspects of energy walls.

1.2 Project Objectives

The scope of this report is the analysis of the effects of seasonal operation of an Energy Wall upon the structure and the soil. This provides an interesting challenge due to the asymmetry of the system, with heat transfer into the soil on one side of the wall only.

Focusing upon the case of the Dean Street Station Box at the Tottenham Court Road Crossrail Station the primary objectives of the project are as follows:

1. Create a two dimensional finite element model of the energy wall at the Dean Street Station Box.
2. Calibrate the parameters governing the behaviour of the soil and the wall by comparing the modelled construction sequence displacement data with displacement data from site.
3. Analyse the effects of the seasonal operation of the energy wall focusing upon:
    - The pore pressures throughout the soil and next to the wall
    - The bending moment within the wall
    - The horizontal displacement of the wall
    - The vertical displacement of the unexcavated soil
    - The effective and total stresses in the soil

The effect of this study is to establish a systematic approach to analysing the effects of the seasonal operation of energy walls. This approach has been mentioned by Arup to form part of a design code which can be used in future studies on energy walls in High Speed 2, Crossrail 2 and in future London Underground constructions.

This will form an important basis on the future of GSHPs and energy foundations within the country as the adoption of energy foundations in the major infrastructure projects act as important case studies for the further development of these systems into new public and private construction projects.

There has been a significant amount of research on various aspects on GSHPs including the effects on the mechanical and thermal properties of soil and on optimisation of the CoP of the GSHPs. There have been a number of studies (Bibliography) on GSHP applications in energy foundations however there has been limited research on the thermo-mechanical response of energy walls to their thermal operation and their affect upon the stresses and displacements of the wall and the surrounding soil. It is important

1.3 Dean Street Station

Crossrail is currently the largest infrastructure project involving the construction of new stations in the United Kingdom. Of the twelve new station boxes ten of them include the installation of Energy Foundations. The Dean Street Station Box which forms the East station box for the Tottenham Court Road Crossrail Station includes energy walls in its design providing 500kW of heating to the station. As part of my initial investigation into this project I arranged a site visit in September 2012, around the time of the final excavation.

Figure 1.3.1 Dean Street Excavation (September 2012)

Situated just North of Soho on Oxford Street the construction programme required a bottom up construction forming one of the deepest open excavations in Europe. The overall construction process creates a space 40x35m plan by 25m deep.

The station consists of a 60m deep and 1m thick diaphragm wall with four 1m thick floor slabs and a 2m thick base slab. The construction sequence originally included five layers of 1m wide steel props throughout the depth of the station, during a site visit in September 2012 we discovered that the lowest steel prop was omitted from the actual sequence in order to reduce the project time. This is due to tight Crossrail Programme times requiring the station to be ready

Figure 1.3.2 Primary Circuit Pipe on the top of Dean Street

for the Tunnel Boring Machine to come through the fully excavated station in 2013.

The installation of the GSHP loops is provided by a separate GSHP contractor during the installation phase of the diaphragm wall reinforcing cage by attaching the pipes to the steelwork. The resulting pipework on the top of the diaphragm wall during construction is incredibly unobtrusive and is evidenced in Figure 1.3.2.

Figure 1.3.4 Cut Piles (September 2012)

Figure 1.3.4 Fifth Prop Location (September 2012)

During the site visit a number of important pieces of information was noted:

1. The fifth prop was removed to reduce project times Figure 1.3.4.
2. The heave reducing piles were cast at the same time as the diaphragm walls and then cut at each stage of the construction Figure 1.3.4.
3. The soil was even less permeable than expected with the sump pumping less water than expected Figure 1.3.6.
4. Lateral displacement data was measured using inclinometers with the wall being fixed in position by surveying the head of the wall Figure 1.3.6.

Figure 1.3.6 Dewatering (September 2012)

Figure 1.3.6 Inclinometer on Diaphragm Wall (September 2012)

1.4 Ground Conditions

The assumed ground stratigraphy of the Dean Street Station Box can be seen in Table 1.4.1.

The original level of the made ground was at 125mATD (metres above the datum), the capping beam for the final station brings the level of the soil up to 126mATD of made ground at the surface of the soil. [6]

Strata	Level of top of layer (mATD)
Made ground (MG)	125
River Terrace Deposits (RTD)	121
London Clay A3 (LC_A3)	117
London Clay A3 (LC_A3)	112
London Clay A2 (LC_A2)	106
Lambeth Group _UMB (LG_UMB)	94
Lambeth Group _LMB (LG_LMB)	86
Lambeth Group _LMB (LG_LMB)	80
Thanet Sand (TS)	74
Chalk	70

Note: Shading denotes material is drained

Table 1.4.1 Ground Stratigraphy

The ground conditions of the site consist mainly of stiff relatively impermeable London Clay and Lambeth Group Clays underlaid by Thanet Sand and Chalk. The entirety of the diaphragm wall is embedded within the low permeability London Clay and Lambeth Group Clays. This means that during the construction process significant excess pore pressures may be developed around and below the toe of the wall which can take a while to dissipate. Being embedded above the sand layer reduces the flow of water which is encouraged by the pressure gradient caused by the removal of the pore water during excavation.

The initial groundwater level is at 120mATD however due to dewatering during the construction process the water level was reduced to the top of the London Clay at 117mATD.

2.0 Theoretical Basis

2.1 Finite Element Model

2.1.1 Model Creation

The 2D mesh was created in Hypermesh with the ABAQUS Standard 2D Interface in

preparation for a custom data file. For the first few weeks we were limited by the delayed renewal of the Hypermesh licence file; however this allowed time to plan the way the mesh would be constructed and organised on paper. I chose to create a separate component for each separable entity organising individual soil layers into assemblies of unexcavated soil, excavated soil behind diaphragm wall, excavated soil inside station and excavated soil behind piles. The boundaries were defined with the middle of the station being one edge allowing for a symmetric analysis to be possible. An arbitrarily distant defined point was used as the far edge and the low

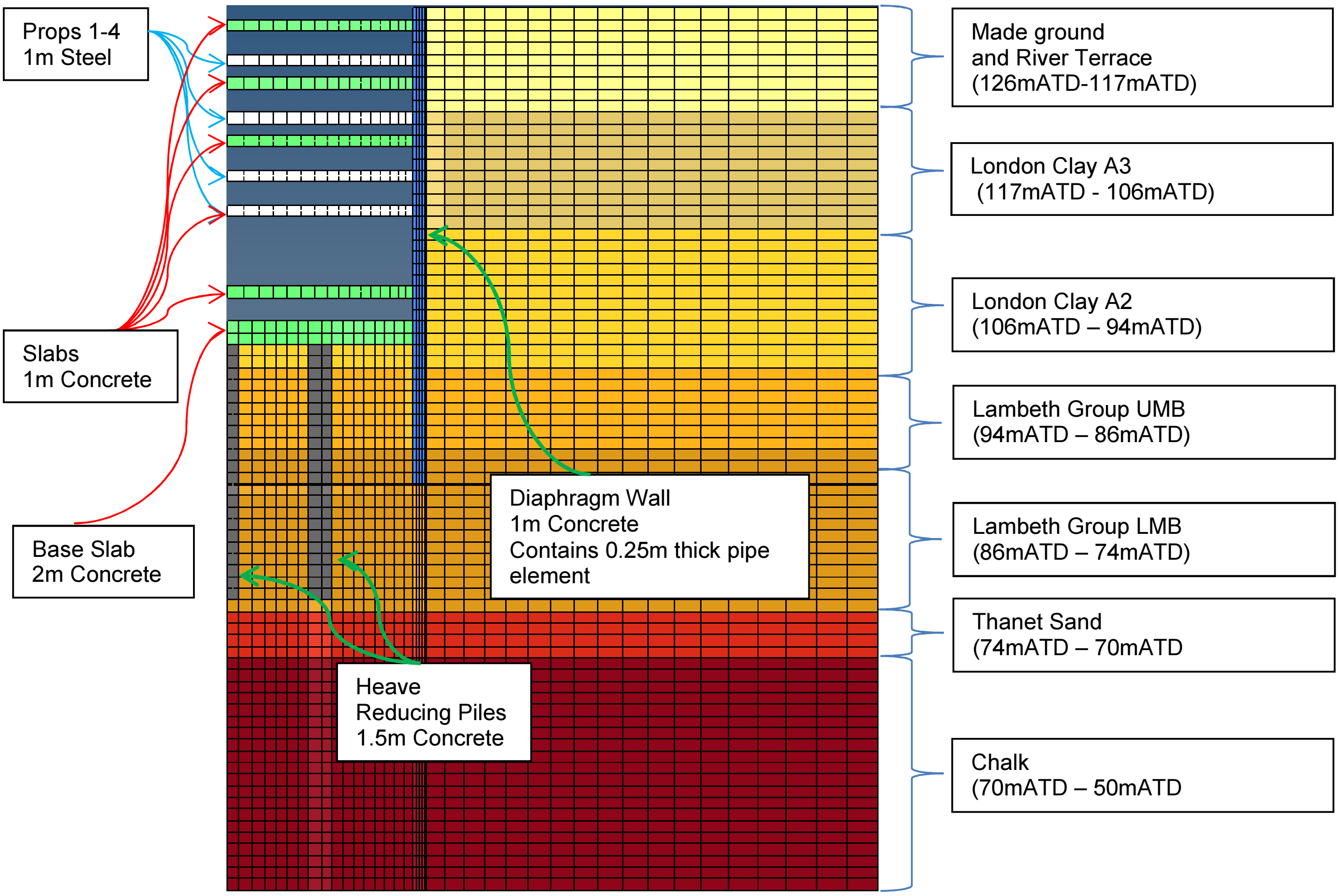

Figure 2.1.1 Hypermesh Model of the Dean Street Station (Omitting 5th Prop)

edge. These points were chosen so as to be far enough away from the station as to be unaffected by the excavation and cycling but close enough to model effectively.

The vertical levels were approximated to 1m element layers to ensure nodal compatibility. The horizontal nodes were defined narrower closer to the diaphragm wall to increase the resolution of the results from 0.4m gaps up to 2m at the far right edge of the model to reduce the number of nodes required. This was necessary to strike a balance between the accuracy and resolution of results and the ability to actually create, maintain and run the analysis in the given timeframe.

The finite element mesh was constructed to take into account not only the finished station but all stages of excavation and construction from the initial undisturbed soil through the bottom-up construction all the way to the finished station box. This involved creating separate components for each soil element in each construction stage, each of these components had to be carefully checked for multiple nodes at the connections between components and then individually exported into solver decks. For each solver deck file the syntax was edited to be consistent with the input required for the finite element software. With over 40 separate files this would have taken quite a while to perform so I employed the use of regular expressions scripting in a text editor which allowed the changes to be made in 4 quick steps. More importantly this reduced the human error of changing the files individually as well as increasing repeatability when more solver decks had to be edited.

The description of each of the component files and of the excavation construction sequence stages was defined in an excel book with material parameters on one sheet and the excavation stages in another sheet. During the analysis a certain number of changes had to occur to the mesh.

These changes included:

- Creating a thin, interface element on the vertical faces of the diaphragm wall as part of the existing soil elements.
- Adding an extra interface element on the toe of the diaphragm wall as part of the existing soil elements.
- Creating individual components for construction stages, not just individual soil layers to be excavated during the analysis.

The 2D mesh was created in Hypermesh with the ABAQUS Standard 2D Interface in preparation for a custom data file. For the first few weeks we were limited by the delayed renewal of the Hypermesh licence file; however this allowed time to plan the way the mesh would be constructed and organised on paper. I chose to create a separate component for each separable entity organising individual soil layers into assemblies of unexcavated soil, excavated soil behind diaphragm wall, excavated soil inside station and excavated soil behind piles. The boundaries were defined with the middle of the station being one edge allowing for a symmetric analysis to be possible. An arbitrarily distant defined point was used as the far edge and the low edge. These points were chosen so as to be far enough away from the station as to be unaffected by the excavation and cycling but close enough to model effectively.

2.1.2 Parameterization

Component Type	Component Name	ID	Original Size (m)	Modelled Size (m)	Original Youngs Modulus (GPa)	Modelled Youngs Modulus (GPa)	Original Poisons Ratio
Temporary Steel	Steel Prop 1	33	0.91	1	210	7.09	0.2
	Steel Prop 2	34	0.91	1	210	7.09	0.2
	Steel Prop 3	35	0.91	1	210	7.09	0.2
	Steel Prop 4	36	0.91	1	210	7.09	0.2
	Steel Prop 5	37	0.91	1	210	7.09	0.2
Permanent Concrete	Diaphragm Wall	8	1	1	28	28	0.2
	Pile 1	22	1.8	2	28	6.785840132	0.2
	Pile 2	23	1.8	2	28	6.785840132	0.2
	Roof Slab	28	0.7	1	28	19.6	0.2
	Level 1 Slab	29	0.7	1	28	19.6	0.2
	Level 2 Slab	30	0.7	1	28	19.6	0.2
	Level 3 Slab	32	0.7	1	28	19.6	0.2
	Level 4 Slab	31	0.7	1	28	19.6	0.2
	Level 5 Slab	27	1.8	2	28	25.2	0.2

Table 2.1.1 Concrete and Steel Properties

The initial soil parameters were taken from directly from the parameters used in Arup's BRICK model and are given in Table 2.1.2. The slabs and props are modelled with different dimensions from the design, especially that of the props, as they are not continuous throughout the section of the wall. The properties for these were determined using transformed sections, by establishing that a dimensionless stiffness must be held constant

This was extended by looking at the actual area and the modelled area a metre deep into the wall to find the stiffness required for the parameterization, the results of this can be found in Table 2.1.1.

The processes to be modelled are the construction sequence to calibrate the model and the seasonal operation of the energy wall over 20 years to determine its effects.

Stratigraphy	Initial stress conditions			Stiffness parameters			Strength parameters			
Stratum	γ (kN/m^3)	K_0 (at top)	K_0 (at base)	E'_v (at top)	E'_v (at base)	Poisson's Ratio '	c' (kPa)	ϕ' (°)	c_u (kPa) (at top)	c_u (kPa) (at base)
Made Ground	18	0.5	0.5	10	10	0.2	0	25	-	-
Terrace Gravel	18	0.5	0.5	25	25	0.25	0	40	-	-
London Clay A3	20	1.2	1.2	24	29	0.2	5	25	104	137
London Clay A3	20	1.2	1.2	29	36	0.2	5	25	137	177
London Clay A2	20	1.2	1	36	49	0.2	5	25	177	250
LG UMB	20	1	1	70	70	0.2	10	28	350	350
LG LMB	20	1	1	70	70	0.2	10	28	350	350
LG LMB	20	1	1	70	70	0.2	10	28	-	-
Thanet Sand	21	1	1	250	250	0.2	0	36	-	-
Chalk	-	-	-	-	-	-	-	-	-	-

Table 2.1.2 Initial Soil Properties

2.1.3 Construction Sequence

In order to accurately model the construction sequence a series of construction stages were introduced and matched as closely as possible with Arup's own design construction sequence. This initially involved creating up to 23 construction stages to be modelled which can be seen in Table 2.1.3 along with the Component ID's that have to be present at each stage. During the FEA this was simplified so that stages 13-23 were condensed into a single stage 13, this was deemed acceptable as there was no more excavation during this time period and only slab casting and depropping occurred in that stage.

Seasonal operation

The seasonal operation of the energy wall at the Dean Street Station are split into two six month cycles annually, a six month Winter station heating (soil cooling) cycle and a six month Summer station recharge (soil heating) cycle. The modelling of the seasonal operation takes place over a 20 year operational life of 20 pairs cycles. The far-field temperature boundary in the soil is kept at 15^{o}C throughout the entire operational life. The operation of the energy wall is to keep the station air temperature at 18^{o}C.

During the Winter cycle the station air is heated to maintain the optimal temperature. In order to maintain this, the GSHP Primary Circuit pumps fluid at 2^{O}C through the pipe in the wall. The model essentially keeps the wall at 2^{o}C throughout the cycle. During Summer the GSHP is put into a recharge state, to maintain 18^{o}C within the station the Primary Circuit is essentially switched off which in the model causes the wall to be held at 18^{o}C throughout the cycle. These operating conditions can be seen in Figure 3.2.1 and Figure 3.2.2.

Stage	Description	Arup Stage	Components Initially Present	Components to remove	Components to introduce
1	Initial Equilibrium		9, 10, 12, 13, 14, 15, 2, 3, 4, 5, 6, 7, 38, 39, 16, 17, 18, 19, 24, 25, 26, 45, 50, 49, 48, 47, 46, 44, 43, 42, 41, 40		
2	Diaphragm Wall Installation		9, 10, 12, 13, 14, 15, 2, 3, 4, 5, 6, 7, 38, 39, 16, 17, 18, 19, 24, 25, 26, 45, 50, 49, 48, 47, 46, 44, 43, 42, 41, 40	All of 9, 10, 12, 13, 14, 15	8
3	Excavate	3	2, 3, 4, 5, 6, 7, 38, 39, 16, 17, 18, 19, 24, 25, 26, 8, 45, 50, 49, 48, 47, 46, 44, 43, 42, 41, 40	40, 46, 16	
4	Install Prop	4	2, 3, 4, 5, 6, 7, 38, 39, 16, 17, 18, 19, 24, 25, 26, 8, 45, 50, 49, 48, 47, 44, 43, 42, 41		33
5	Excavate		2, 3, 4, 5, 6, 7, 38, 39, 16, 17, 18, 19, 24, 25, 26, 8, 33, 45, 50, 49, 48, 44, 43, 42	17, 41, 47	
6	Install Prop	5	2, 3, 4, 5, 6, 7, 38, 39, 18, 19, 24, 25, 26, 8, 33, 45, 50, 49, 48, 44, 43, 42		34
7	Excavate		2, 3, 4, 5, 6, 7, 38, 39, 18, 19, 24, 25, 26, 8, 33, 34, 45, 50, 49, 48, 44, 43, 42	42, 48	
8	Install Prop	6	2, 3, 4, 5, 6, 7, 38, 39, 18, 19, 24, 25, 26, 8, 33, 34, 45, 50, 49, 44, 43		35
9	Excavate		2, 3, 4, 5, 6, 7, 38, 39, 18, 19, 24, 25, 26, 8, 33, 34, 35, 45, 50, 49, 44, 43	43, 49	
10	Install Prop	7	2, 3, 4, 5, 6, 7, 38, 39, 18, 19, 24, 25, 26, 8, 33, 34, 35, 45, 50, 44		36
11	Excavate		2, 3, 4, 5, 6, 7, 38, 39, 18, 19, 24, 25, 26, 8, 33, 34, 35, 36, 45, 50, 44	18, 44, 19, 50	
12	Cast Base Slab	9	2, 3, 4, 5, 6, 7, 38, 39, 24, 25, 26, 8, 33, 34, 35, 36, 45		27
13	"Pile Installation"		2, 3, 4, 5, 6, 7, 38, 39, 24, 25, 26, 8, 33, 34, 35, 36, 27	All of 24, 25, 26	22, 23
14	Remove P4	11	2, 3, 4, 5, 6, 7, 38, 39, 8, 33, 34, 35, 36, 27, 22, 23	36	
15	Cast Level 3 Slab	12	2, 3, 4, 5, 6, 7, 38, 39, 8, 33, 34, 35, 27, 22, 23		32
16	Remove P3	14	2, 3, 4, 5, 6, 7, 38, 39, 8, 33, 34, 35, 27, 22, 23, 32	35	
17	Cast Level 2 Slab	15	2, 3, 4, 5, 6, 7, 38, 39, 8, 33, 34, 27, 22, 23, 32		30
18	Cast Level 4 Slab	15	2, 3, 4, 5, 6, 7, 38, 39, 8, 33, 34, 27, 22, 23, 32, 30		31
19	Remove P2	21	2, 3, 4, 5, 6, 7, 38, 39, 8, 33, 34, 27, 22, 23, 32, 30, 31	34	
20	Cast Level 1 Slab	22	2, 3, 4, 5, 6, 7, 38, 39, 8, 33, 27, 22, 23, 32, 30, 31		29
21	Remove P1	23	2, 3, 4, 5, 6, 7, 38, 39, 8, 33, 27, 22, 23, 32, 30, 31, 29	33	
22	Cast Roof Slab	24	2, 3, 4, 5, 6, 7, 38, 39, 8, 27, 22, 23, 32, 30, 31, 29		28
23	Final Construction		2, 3, 4, 5, 6, 7, 38, 39, 8, 27, 22, 23, 32, 30, 31, 29, 28		

Table 2.1.3 Construction Sequence

2.2 Finite Element Analysis (FEA)

2.2.1 Theoretical Basis

The finite element analysis is being conducted using a non-commercialised piece of software being developed by Cambridge University Engineering Department. The software is specifically designed for the analysis of soil mechanics using both an undrained and drained Coulomb model as well as a fully coupled Thermo-Hydro-Mechanical analysis for the seasonal operation of the energy wall.

Mass Continuity

$$\frac{\partial \rho}{\partial t} = \Delta.(\rho \boldsymbol{v}) = 0$$

Energy Conservation (for each single-phase material)

$$\frac{\partial(\rho c_p T)}{\partial t} + \Delta.(\rho c_p T \boldsymbol{v}) = \Delta.k\Delta T + H$$

Momentum Conservation

$$\frac{\partial(\rho \boldsymbol{v})}{\partial t} = \Delta.(\rho \boldsymbol{v}^2) = \Delta.\boldsymbol{\sigma} + \rho \boldsymbol{g}$$

ρ is density, **v** is a velocity vector, t is time, **g** is the vector for acceleration due to gravity, **σ** is the stress tensor in the material, k is the thermal conductivity, T is the temperature, c_p is the specific heat at constant pressure, and H represents the heat input from all sources.

Soil Characterisation

The soil is characterised by a Mohr-Coulomb model that expresses stresses as a function of strains. The soil follows the Terzaghi's principle of effective stresses:

$$\sigma = \sigma' + u$$

Where σ is the total stress, σ' is the effective stress and u is the pore pressure.

Pore Fluid Characterisation

The pore fluid is incompressible and is assumed to flow following Darcy's Law:

$$q_h = -k_h \Delta H$$

Where q_h is the flow per unit area, k_h is the permeability of the soil, and ΔH is the vector of the hydraulic gradient driving the fluid.

Heat Transfer Mechanisms

For this project only conduction and convection are modelled as they contribute the most towards the heat transfer. As the pore pressure variation is small and the soil is incredibly impermeable conduction dominates as the main heat transfer mechanism. Heat conduction follows Fourier's Law:

$$q_T = -k_T \Delta T$$

q_T is the heat flow per unit area, k_T is the thermal conductivity and ΔT is the vector of the thermal gradient driving the fluid.

Volumetric Strains in Soil and Pore Fluid

Taking compression as positive, the volumetric strain the soil structure is governed by a function composed of three terms:

1. Contribution due to stress changes in the soil structure in three dimensions.
2. Contribution from the soil skeletal expansion due to soil grain expansion.
3. Contribution from the soil structure shrinkage due to structure collapse.

$$\epsilon_{v(skeleton)} = tr[D^{-1}(d\sigma - dp)] - \alpha_{s-g} dT$$

Where T is the temperature, α_{s-g} is the thermal expansion coefficient of the soil grains, α_{s-s} is the thermal contraction coefficient due to the collapse of the structure, σ is the soil stress, p is the pore pressure, D is the stiffness matrix and tr indicates that the volumetric strains are calculated as a function of varying effective stress and pore pressure.

Volumetric strain is a function of the thermal expansion of the fluid:

$$\epsilon_{v(porewater)} = -n\alpha_w dT + \frac{n}{K_w} dp + q_w$$

Where T is the temperature, n is the porosity, α_w is the thermal expansion coefficient of pore water, K_w is the bulk modulus of the pore water, p is the pore pressure and q_w is the flow of pore water out of the pores per unit area (q_w=0 when undrained).

$$tr[D^{-1}(d\sigma - dp)] - \alpha_{s-g}dT + \alpha_{s-s}dT = -n\alpha_w dT + \frac{n}{K_w}dp + q_w$$

$$tr[D^{-1}(d\sigma - dp)] + \frac{n}{K_w}dp + \left(n\alpha_w - \alpha_{s-g} + \alpha_{s-s}\right)dT = q_w$$

Fully coupled Thermo-Hydro-Mechanical (THM) Analysis

In order to analyse the effects of the seasonal thermal operation of the energy wall a coupled THM analysis is used, the governing equations are [7]:

$$\begin{cases} \partial^T [D]\left([\partial]\{r\} - \{\varepsilon^H\}\right) + \nabla p = F_1 \\ \nabla^T \left[k\right] \nabla p + \nabla^T \dfrac{dr}{dt} + \dfrac{1}{k_w}\dfrac{\partial p}{\partial t} - n\alpha_w \dfrac{dT}{dt} = F_2 \\ \rho_w c_p \dfrac{\partial}{\partial t} T - \nabla^T D \nabla T - c_p^w k_h \nabla^T (T\nabla p) = F_3 \end{cases}$$

Where $\{d\epsilon\}^H = \alpha[1\ 1\ 1\ 0\ 0\ 0]^T dT$ and δ is the displacement. The other variables have been described for previous equations. This system of couple equations is solved using the software being developed in Cambridge University Engineering Department called openFTL/geoKit (Rui. Y, 2013).

2.2.2 Analysis

Numerical Integration openFTL/geoKit

openFTL/geoKit performs Gauss Point numerical integration using the theory established above assuming that the displacements are small. The computation was carried out by the developer of the code, Yi Rui. The basis of this code can be found in [7].

Paraview

Once the FEA was complete the data was viewed in Paraview, an open-source data visualizer. Figures such as Figure 3.1.1 were generated using Paraview. Using Paraview data over lines could be extracted and were exported for all timesteps into csv files. Paraview is not ideal though; it crashes a lot and is not designed for viewing data where there are multiple component files with a construction sequence that requires components to be masked. In future research it is worth pursuing better data visualisation software or to do all of the work using Matlab.

Matlab

The detailed data analysis was processed in Matlab. One of the limitations of Paraview is that it produces .csv files with strings, and for each timestep (of which there are 252) it produces a separate file. As a result, in order to process the data into csv files which are readable takes Matlab two hours to complete before any data can be processed. Due to delays in the FEA process the Matlab code was developed during the FEA process. As a result, when the final data was available for processing on 21/5/2013 the data was analysed and visualised very quickly as the code had already been produced and bugs had already been fixed.

2.2.3 Analysis change from original plan

During the FEA procedure a number of changes occurred from the original plan in order to simplify the procedure:

- The wall elements were not replaced with a concrete wall component but the properties were instead changed to those of concrete at wall installation stage.
- The heave piles were not included in the construction sequence modelling; this was due to them not having a significant effect upon the geotechnical properties that were being modelled.
- The soil interface elements were not individually modelled as having separate stiffness depending on which soil layer they were in, this was again in order to simplify the model as they had little effect upon the geotechnical properties that were being modelled.
- The data from the model at each timestep is at the end of each stage and not at the beginning, as a result the initial data for each step must be taken from the stage before, this is visualisation and processing of the results.

3.0 Results and Discussion

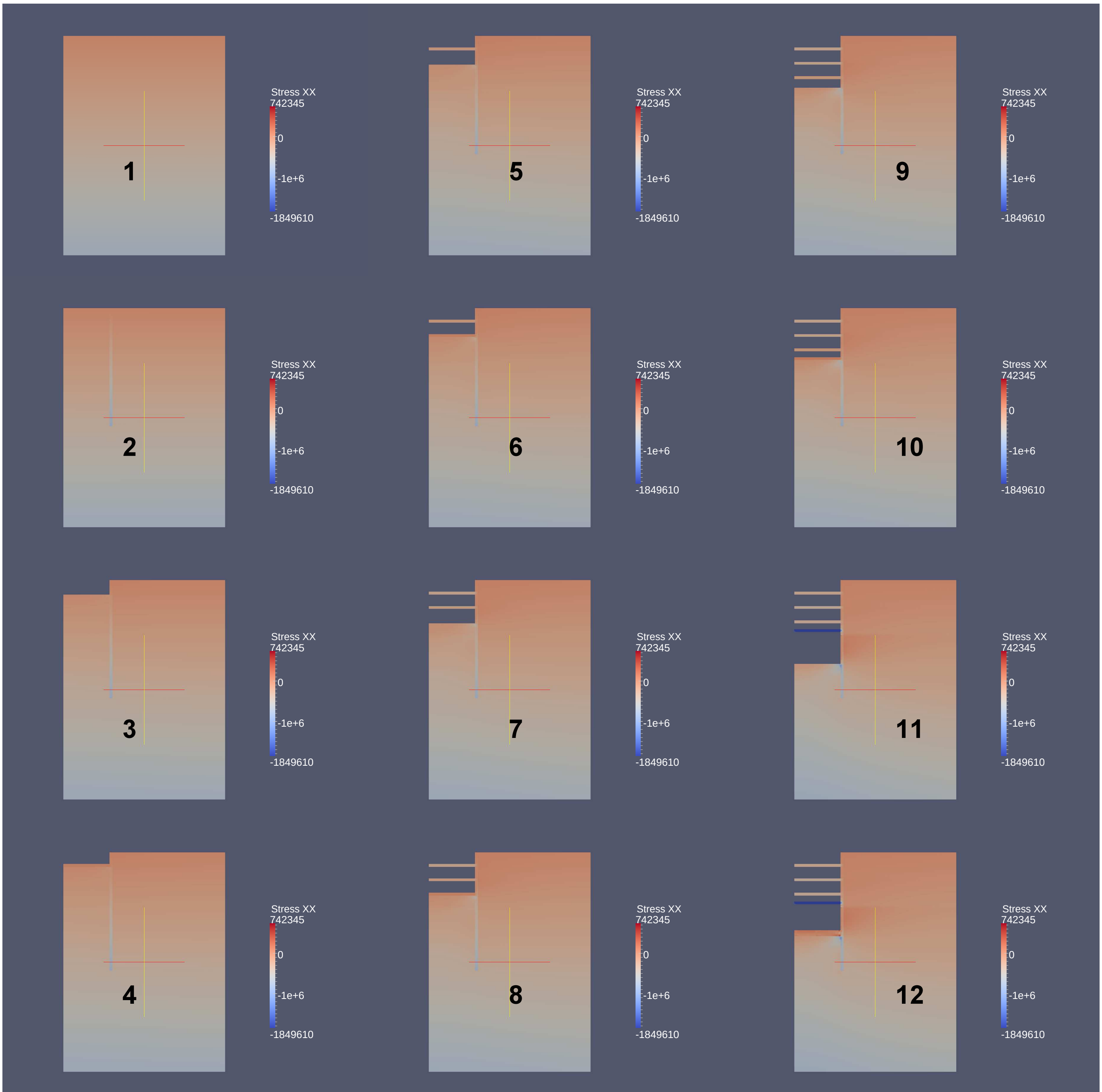

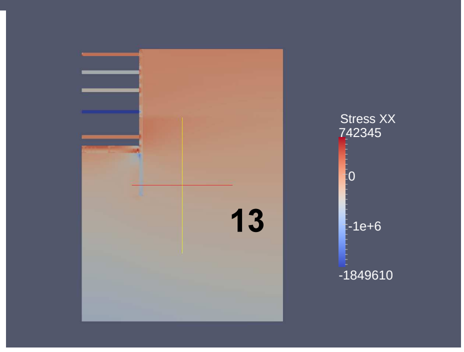

Figure 3.1.1 Construction Sequence Stages 1-13 in Paraview (Section 2.1.3)

3.1 Construction Sequence

The construction sequence described in Section 2.1.3 was modelled using the openFTL//geoKit software, the results were viewed in Paraview, which was then exported to csv files for processing in Matlab.

3.1.1 Horizontal Displacement

The construction sequence was primarily modelled in order to calibrate the stiffness of the soil. This was an iterative process which involved increasing the stiffness to reduce the magnitude of the displacements until they were acceptably similar to the displacements on site. The development of the model can be seen in figure 3.1.1 which shows the modelled displacements for the last three iterations of the model before a model was deemed acceptable.

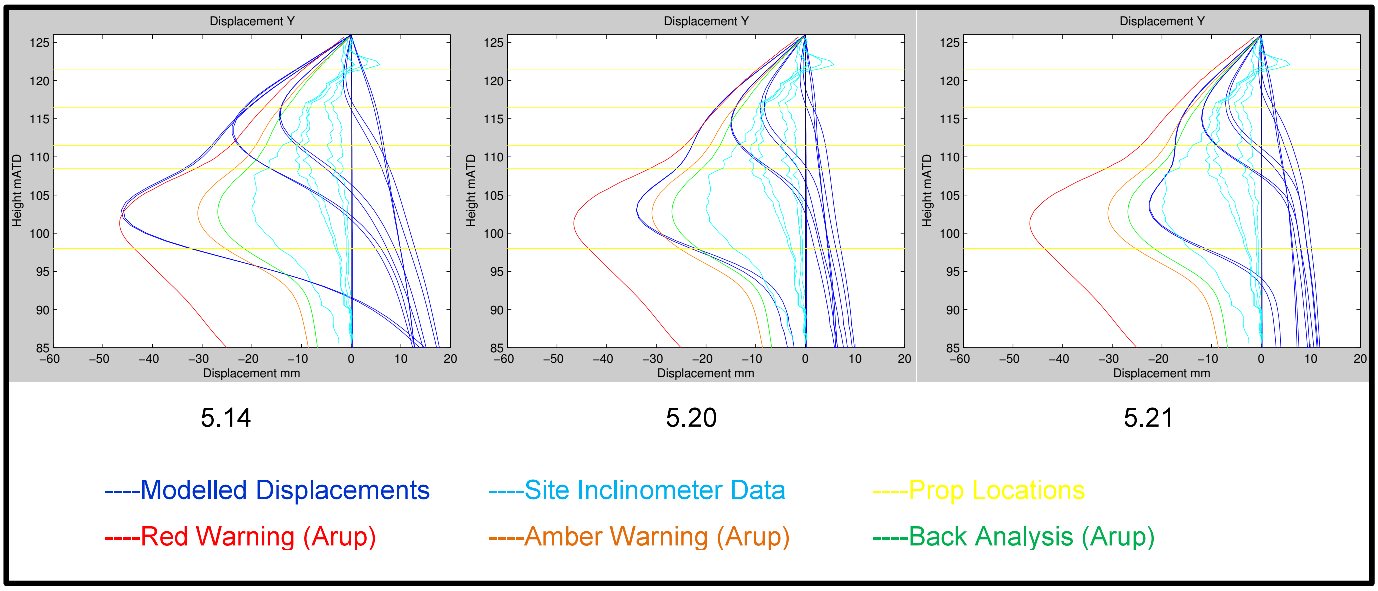

Figure 3.1.2 Displacement of the wall during construction (negative is into the station)

In order to calibrate the model the dark blue line of the modelled displacements needed to be as close as possible to that of the light blue inclinometer site data. This progression of displacement results allowed model 5.21 to be chosen.

The displacement of the wall and soil are caused by changes in the pore pressure and by thermal expansion and contraction. During the construction stages the temperature is held constant so all displacement effects are all due to the changes in pore pressure. As the data in Figure 3.1.2 shows, as the excavation progressed the displacement increased with the maximum horizontal displacement being just above the level of the excavation. This is because, as the soil is excavated there is progressively less and less passive stress to hold the soil back, this is mitigated by the installation of props. The props have a much lower area than the excavated soil, thus have a lower dimensionless stiffness than the soil. As more and more soil is excavated the total relative stiffness provided by the props becomes less and less than the excavated soil, this means that the further the excavation progresses the greater the overall displacements.

The maximum displacement of the soil from model 5.21 was -25mm and from site data this was -20mm. The magnitude and shape of this data was deemed to be a close enough approximation of the site inclinometer data to be used to model both the construction sequence and the seasonal operation of the energy wall. The final and originally modelled stiffness of each component are given in Table 3.1.1. These are the governing factor which changed the way the soil displacement behaved, as such all the other material parameters are the same as those given in Table 2.1.2 and Table 2.1.1.

Soil	Original Stiffness (Mpa)	Final Model Stiffness (Mpa)
Made Ground	10	40
Terrace Gravel	25	50
London Clay A3	24	72
London Clay A3	29	147
London Clay A2	36	210
Lambeth Group UMB	70	210
Lambeth Group LMB	70	250
Lambeth Group LMB	70	250

Table 3.1.1 Original input stiffness alongside final model stiffness

The modelled displacements shown in Figure 3.1.2 show large lateral movement at the toe of the wall into the unexcavated soil, this was done due to the way the site inclinometer data was measured on site. As mentioned earlier inclinometers can be analysed to give a displacement relative to the head or toe of the wall, Arup surveyed the head of the wall at each stage to account for the bulk movement of the wall, in order to match Arup's data the modelled displacement data for the purposes of calibration also took the displacement at the head of the wall as zero.

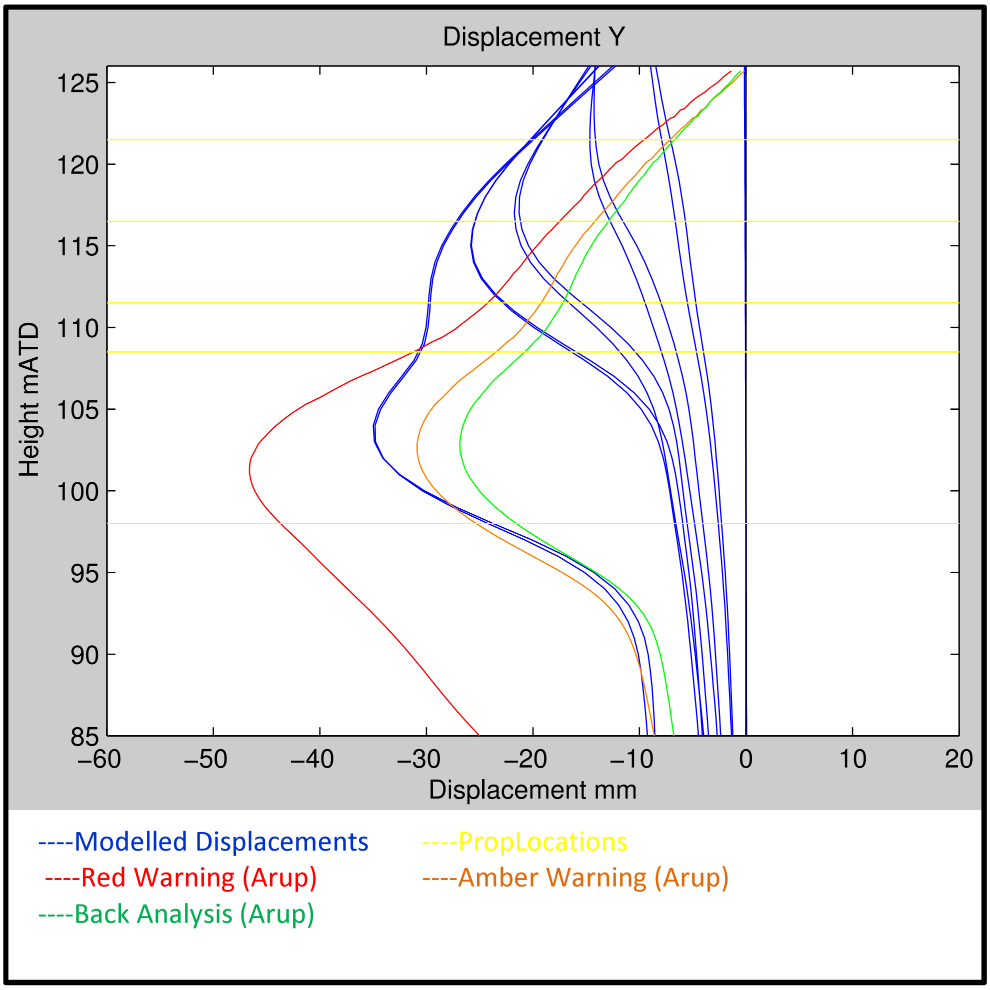

Figure 3.1.3 Raw Displacement data of the wall during construction (negative is into the station)

Figure 3.1.3 shows the raw displacement data without fixing the head of the wall to match the inclinometer data, it can be seen that as soon as the wall is installed a large lateral displacement into the station occurs, this is due to the assymetric nature of the model, which causes the wall to lean towards the smaller side of the model. Fixing the head of the wall allows the data to be compared to the inclinometer data, the leaning nature of the wall causes the large lateral displacements at the toe of the wall when the head is fixed at 0 as was seen in Figure 3.1.2. In order to revise this further work must be done to prevent the model from being sensitive to the assymetry.

Due to the way the model portrayed the construction sequence, the effect of consolidation on the displacement of the wall can be seen from the timestep between excavation to a certain level and the next timestep which is the installation of the prop (such as 7 to 8). The model was limited as the timesteps were constant and did not reflect the real timescales of construction; further study needs to be undertaken to rectify this problem. This does provide an insight into how the consolidation affects the displacement. Figure 3.1.4 shows us that the effect of consolidation reduces the magnitude of the displacement into the wall. The blue line shows the displacement of the wall immediately after excavation and the red line shows the displacement one timestep later when the prop is installed. For construction stages 7 to 8 the displacement into the station reduced by 0.5mm at the

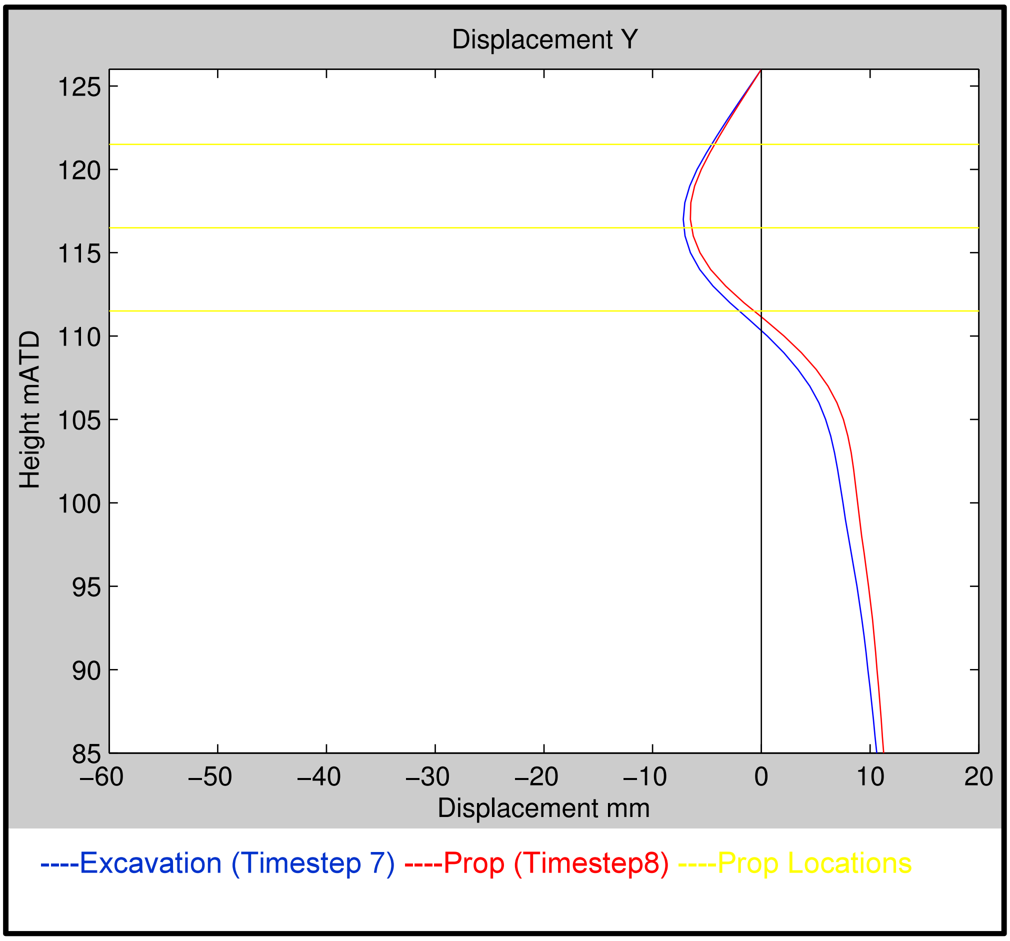

Figure 3.1.4 Displacement of the wall during excavation to 111mATD and installation of Prop 3

maximum point from -7mm to -6.5mm. This suggests that, even if the timesteps are inaccurate or if the permeability is too high in the model the model is still conservative as the displacements reduce due to consolidation over time.

3.1.2 Pore Pressure

The pore pressure variation during the stages of construction are very small compared to the baseline, these can be seen throughout the soil Figure 3.1.5. In order to compare this it is far easier to look at the variation in excess pore pressure during the stages of construction which are summarised in Figure 3.1.6. It can be

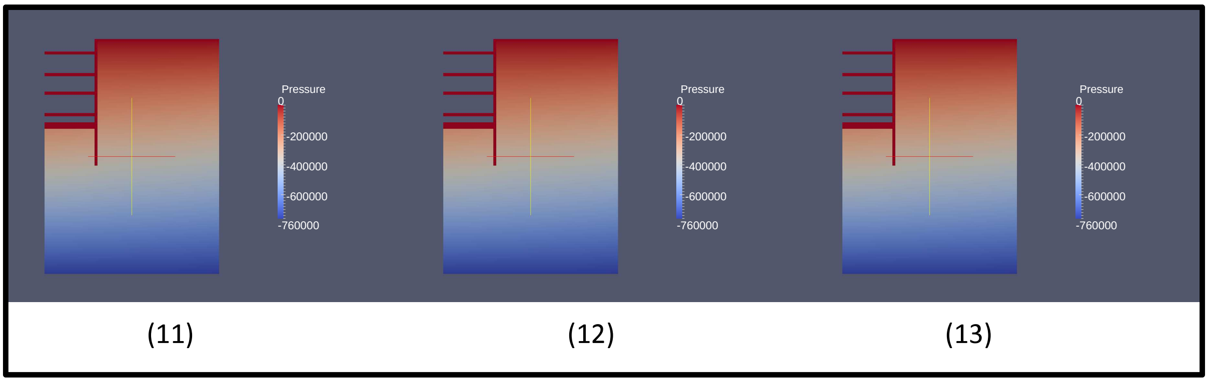

Figure 3.1.5 Pore pressure development during the final stage of construction (in Pascals)

seen in the figures after each stage of excavation a negative excess pore pressure develops on the unexcavated side of the wall. As the soil is excavated the soil beneath the excavation has its total vertical stress acting on it reduced, by virtue of the load being removed. As the soil is undrained the effective stress in the soil initially remains constant so a negative excess pore pressure must be generated to cause this due to Terzaghi's Principal.

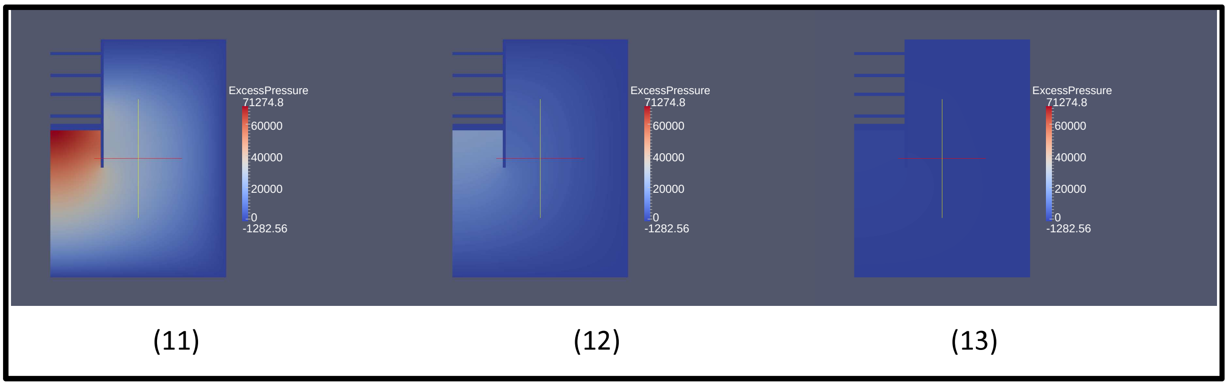

Figure 3.1.6 Excess pore pressure development during the final stage of construction (in Pascals)

During consolidation the total stress remains constant and the excess pore pressures dissipate to return to their in situ values (thus causing Effective Stress to reduce, see Section 3.1.4). This is clearly demonstrated in Figure 3.1.6 and Figure 3.1.5 where timesteps 11-13 show an excess pore pressure of about -60kPa form at the surface of excavation (99mATD) on the station side of the soil and an excess pore pressure of about -40kPa develop at a slightly lower point (80mATD) on the unexcavated side of the wall. As the timesteps progress these excess pore pressures dissipate due to consolidation, whereby the pore fluid flows through the low permeability clay over a period of time to dissipate the pore pressures generated.

With the highly impermeable nature of the London Clay and the Lambeth Group it is highly unlikely that consolidation will actually be completed in the 15 days modelled. This is however a much smaller space of time than actually than is actually seen on site. This is a limitation of the model and further studies must be conducted in order to make this simulate the correct timescales for consolidation during construction.

3.1.3 Total and Effective Horizontal Stress

The effective and total horizontal stresses in the soil are of utmost importance to the analysis on the effects of the construction and seasonal operation of the soil as they cause bending moments to be generated within the wall.

As has been discussed previously about pore pressures when an amount of soil is excavated the total vertical stress is reduced, this similarly means that the total horizontal stress is also reduced. By virtue of the undrained behaviour of the soil the effective stresses remain constant at the moment of excavation and negative pore pressures are generated to account for the balance Terzaghi's Principal

This suggests that when soil is excavated there will be an immediate drop in total horizontal stress in the soil below the excavation but the effective horizontal stress initially remains constant. As time passes for consolidation the total horizontal stress should remain constant and the effective stresses should decrease to mirror the

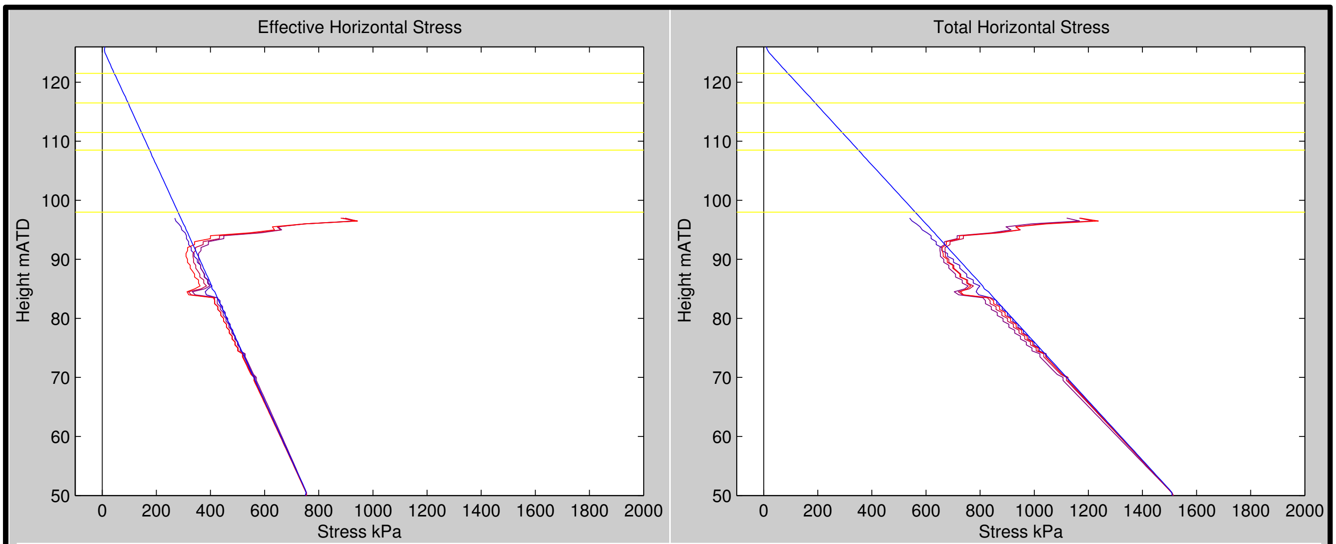

(a) (b)

----Initial Conditions (Timestep1) ----Prop 4 (Timestep 10) ----Final Excavation (Timestep11)

Figure 3.1.7 Effective(a) and Total Horizontal Stress(b) during construction on the Station Side

dissipation of negative pore pressures described in section3.1.2 .

Figure 3.1.7 and Figure 3.1.9 show the how the total and effective horizontals develop from a the initial conditions to the effects of an excavation. Prop 4 is used to show the stresses just before excavation as well as showing the effects of in reducing the horizontal effective stresses over time.

As the pore pressure that were generated by the model were so small the changes in effective stress and total stress are hard to determine by inspection of Figure 3.1.6 and Figure 3.1.5. It was however easy to verify that the model did measure this accurately by directly comparing the data for the effective stress, pore pressure and the computed total stress. This was fairly straightforward and showed that the model was acceptable and obeyed that total stress is equal to effective stress vs pore pressure. It can be seen that the effective stresses reduce as the timesteps increase in both figures.

At the top of the soil near the excavation in Figure 3.1.7 a large horizontal effective stress develops because the soil is no longer confined from above and the wall displaces inwards at this point which puts large horizontal stresses into the soil which are seen in the figure.

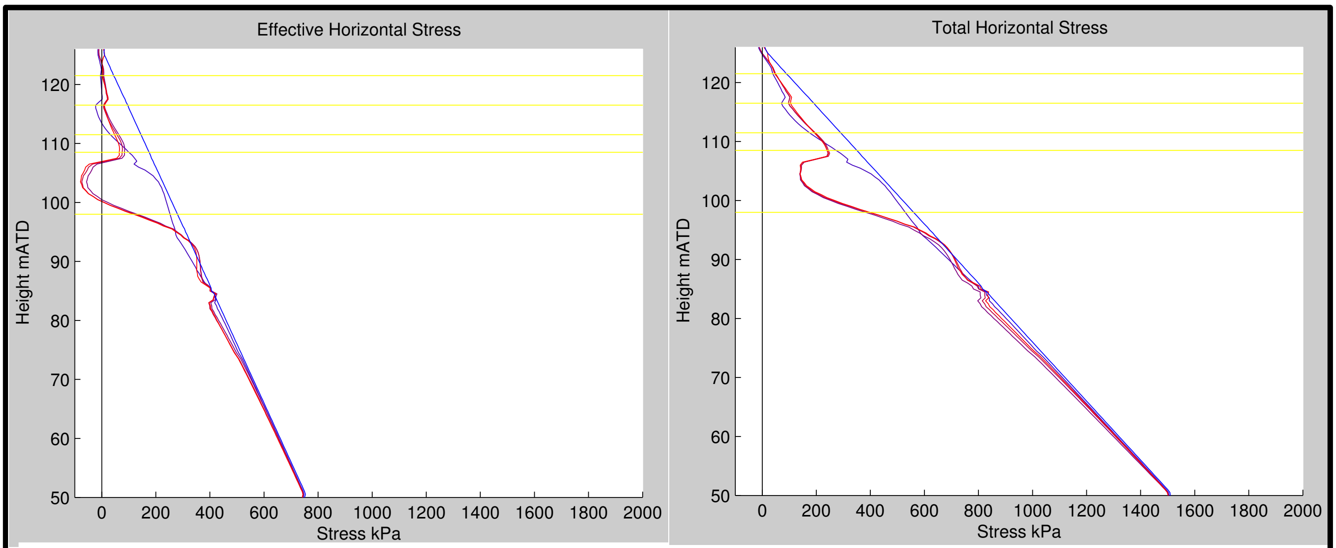

(a) (b)

----Initial Conditions (Timestep1) ----Prop 4 (Timestep 10) ----Final Excavation (Timestep11) ----Base Slab Cast (Timestep12) ----Construction Complete (Timestep13) ----Prop Locations

Figure 3.1.8 Effective(a) and Total Horizontal Stress(b) during construction on the Unexcavated Side

On the station side of the wall the behaviour is fairly straightforward as the soil is being directly unloaded and the behaviour seen in Figure 3.1.6 is expected. The stress behaviour on the unexcavated side of the wall differs from this. The excavation being shown is to the final depth at 97mATD. The horizontal stresses in the unexcavated section mimic the displacements of the wall, as the wall displaces this allows the soil to expand thus reducing the total and therefore effective stresses in the wall to a similar shape of the excavation that occurs. As the fifth prop is no longer present in the actual construction of the station box, the largest displacement and therefore the largest reduction in total and effective horizontal stresses are likely to be seen in the span between the fourth prop and the base slab, an effect which can be seen both here in Figure 3.1.5 as well as in the displacement Figure 3.1.4 for a different excavation stage. As the total pore pressures are always positive the effective stress is always less than that of the total stresses in the construction.

Figure 3.1.8(a) presents an impossibility of a negative effective stress, in reality the stress here would be zero however the Mohr-Coulomb model includes a cohesion constant which can technically give a negative effective stress as a result. Further study using a more advanced Mohr-Coulomb code is required to account for this problem.

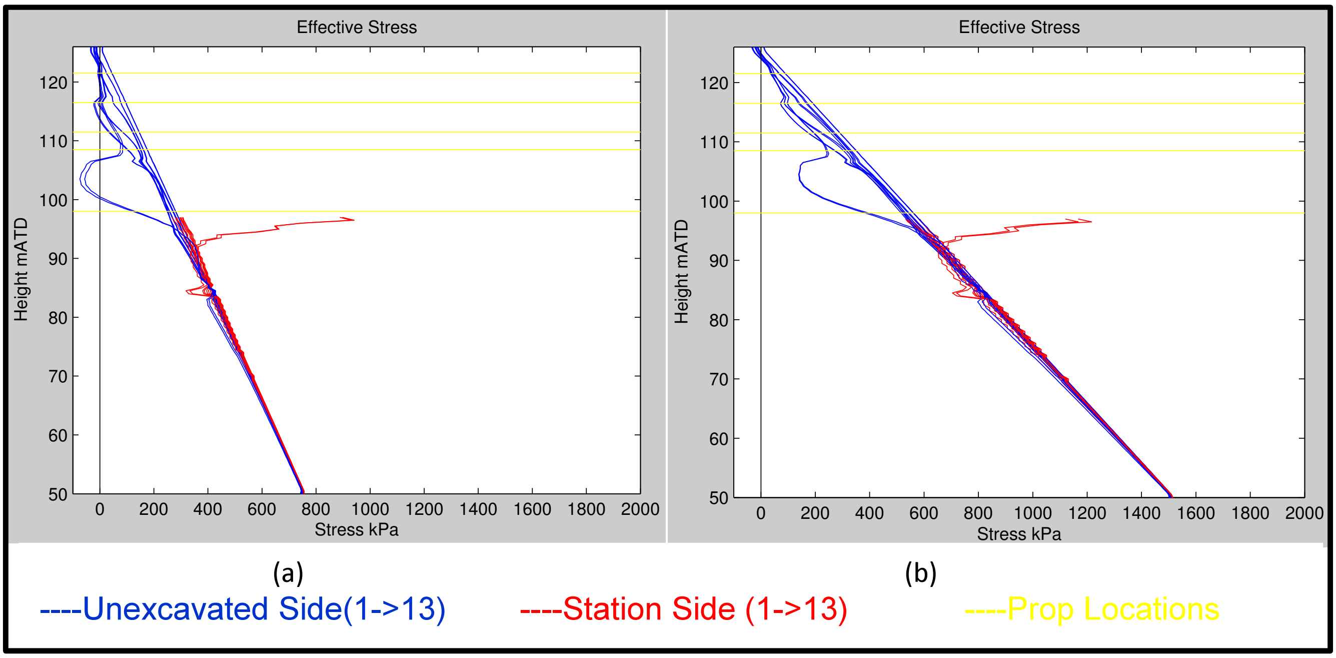

Figure 3.1.9 Effective(a) and Total Horizontal Stress(b) during construction

Figure 3.1.9 shows the Total and Horizontal Stresses for every construction stage from the initial conditions all the way to the final station with cast concrete slabs. The blue data represents the data from the unexcavated soil side and the red data shows the data from the station side of the wall. It is important to note that as the excavation progresses the total and effective stresses reduce near the surface of the soil, the effective stresses consolidate back to their original position very quickly, this is a limitation with the current model and is something that would require further study to determine the effects of this. The effects of the consolidation are possible to see in Figure 3.1.7, Figure 3.1.8 and Figure 3.1.9 where the change in the effective stress after each timestep can be seen to be greater than that of the total stress.

It is important to note that as the effective and total stresses change on either side of the wall they move to balance the forces affecting the wall, reducing its overall movement. What cannot be seen are the forces from the props adding to the passive restraining pressure from the soil on the station side of the wall. The balance of the two forces prevents the wall from failing catastrophically due to soil failure, by inspection of the Figure 3.1.9 it may seem that this does not satisfy that but the stresses from the soil are not displayed here, again a limitation of the model however it was possible to verify that this was indeed the case by integrating the stresses and forces at each timestep to check the forces balance.

3.1.4 Bending Moment in the Energy Wall

The changes in stresses and strains in the soil adjoining the diaphragm wall due to the construction and seasonal operation of the energy wall and the time effects of consolidation cause bending moments to be generated throughout the depth of the wall. As the soil is excavated and the props are installed the pressures and stresses acting on both sides of the wall change which induce varying strains throughout the section of the wall inducing changes in bending moment, as consolidation progresses the pore pressure rises which causes the effective stresses to drop also causing the strains in the wall to vary causing the bending moment to change.

The bending moment variation throughout the depth of the wall can be ascertained by taking the normalized vertical stress at various points through the section of the wall for a unit width of the wall and multiplying this by the distance to the centre of the wall. To account for variations in this the average value for four points through the section of the wall at every metre depth of the wall was taken to find a more accurate estimate for the bending moment variation.

The variation in bending moments in the wall are plotted against the bending moment envelopes provided by Arup during their BRICK modelling on the original construction seqeunce. As such the envelopes still include the effects of a the fifth prop. As the actual construction skips the fifth prop the modelled construction also does this to simulate the construction. Therefore we expect that the bending moment between the fourth prop and the base slab is likely to be larger and the maximum point likely to be deeper than envelopes. This is characterised in Figure 3.1.10 which shows the plot, the final levels of construction follow the shape of the bending moment envelopes quite well whilst staying within the maximum bounds the envelope sets. The large bending moments at 95mATD, 102mATD and 107mATD are the evidence of this, although they are at a lower point than expected. This result

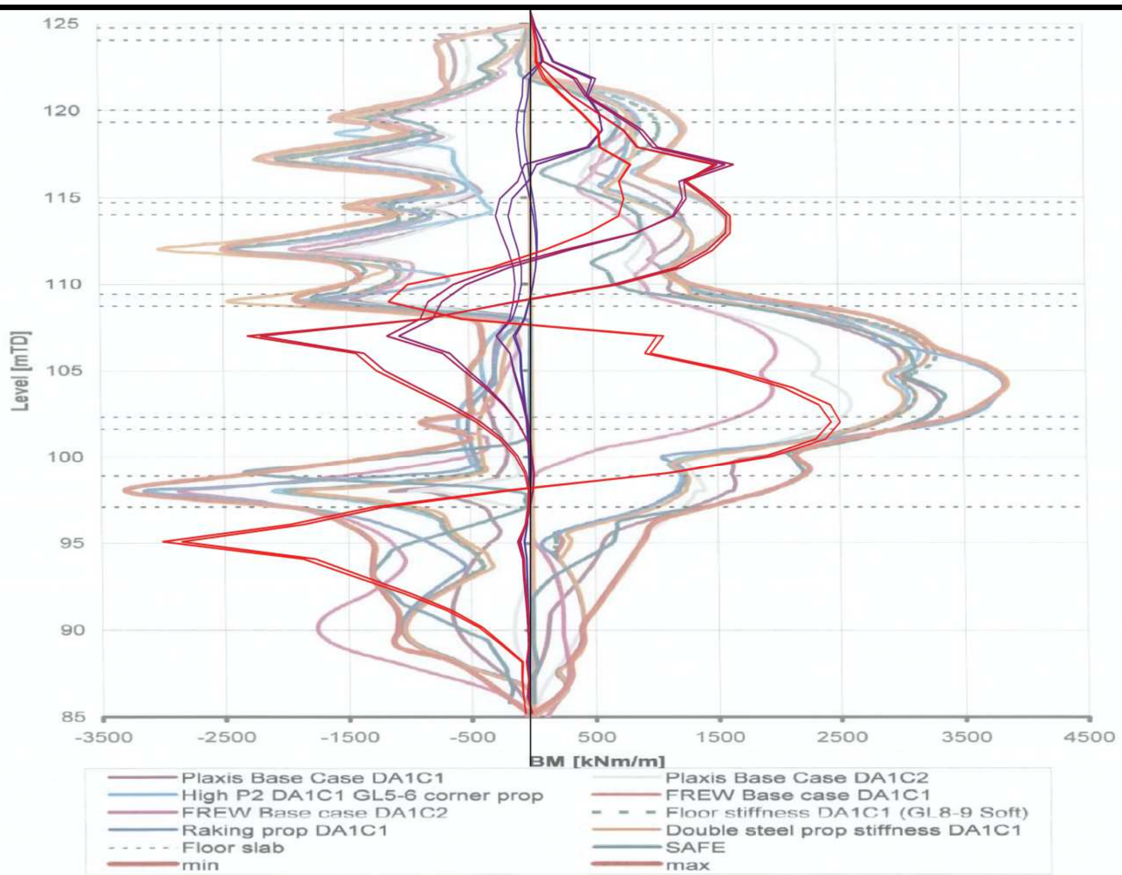

----Bending Moment (Timestep 1) Varies in colour corresponding to timestep

----Bending Moment (Timestep 12)

Figure 3.1.10 Bending Moment in Wall During Construction with Arup envelopes

appears to be from complications in the development of the openFTL/geoKit software and further work will need to be done to refine the result.

Taking the cross section of wall of unit depth we can calculate the plastic moment capacity of the wall as:

$$M_P = \frac{bd^2}{4}\sigma_y = \frac{1 \times 1^2}{4} \times 30MPa = 7.5kNm$$

This gives a maximum boundary for the ultimate bending moment capacity of the wall and we can see that both the envelope and the modelled bending moment are much smaller than this.

3.1.5 Surface Settlement

Due to the location of the Dean Street Station Box, the excavation is surrounded on all sides by buildings less starting less than five metres from the edge of the excavation, differential settlement can cause serious problems to the buildings in the

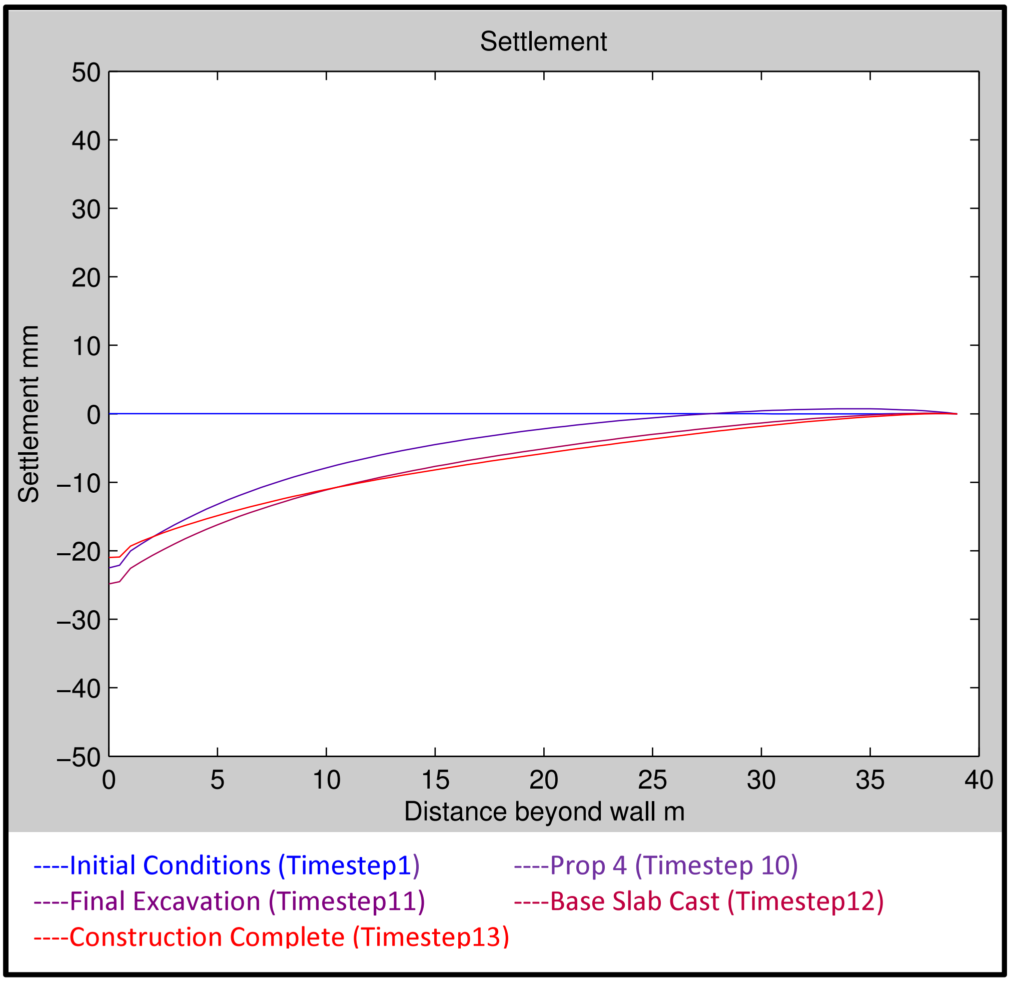

Figure 3.1.11 Surface Settlement of soil beyond the wall

area. Figure 3.1.11 shows the surface settlement from the initial preconstruction stages to the final excavations stages with the effects of consolidation. As consolidation occurs the negative pore pressure dissipate by drawing in pore fluid, this causes the ground to swell thus reducing the surface settlement, this is clear to see in Figure 3.1.11 showing Timestep's 12 and 13 when no more construction had occurred.

The change in gradient of settlement is not very severe beyond five metres from the edge of the wall. The model does not account for the presence of a TAM grouting procedure at the site during both the excavation sequence and the tunnelling sequence, this suggests that the surface displacements seen here are grossly conservative, as such the importance of looking at the surface settlements during the construction process are not to establish their effect on the buildings but to establish a baseline to look at the effects on settlement from the seasonal operation of the energy wall.

3.1.6 Summary of Construction Sequence

The analysis of the Construction Sequence allowed the model to be calibrated in order to better simulate the geotechnical behaviour of the soil and the structural behaviour of the wall and props. It allowed a baseline to be established in order to compare the relative changes in these properties due to the seasonal operation of the Ground Source Heat Pump. Of course, in order to establish a more thorough model the code could be further refined to account for location of the maximum bending moments and to compare the bending moment envelope with a revised design bending moment envelope from Arup which accounts for the lack of the fifth prop.

3.2 Seasonal Operation

The effects of the seasonal operation of the ground source heat pump and its effects upon the displacements, bending moments, stresses and pressures in the soil are the focus of this study. The seasonal operation was analysed in blocks of six month long timesteps for both the Winter Heating (Soil Cooling) Cycle and the Summer Cooling (Soil Heating) Cycle for 20 years of continuous operation to look at the long term effects on the wall and the soil.

3.2.1 Temperature within the soil

The seasonal operation of the energy wall is most readily seen in the temperature variation throughout the soil during the Winter Soil Cooling and Summer Soil Heating Cycles. The model is 12^{o}C lower than the actual operating conditions, so the upper limit of 6^{o}C equates to the actual operating temperature of 18^{o}C. As the model does not account for phase changes of the pore fluid it is just a simple case of changing the scales to see the effects as ground freezing is not an issue in the model.

The variation of temperature throughout soil during the Winter cycle can be seen in Figure 3.2.1 and the Summer cycle can be seen in Figure 3.2.2. It is clear that the heat transfer through the soil is sufficiently small as to not cause significant temperature changes far from the wall even over a six month heating or cooling cycle. As can be seen the temperature variation does not affect the soil more than 5m away, which remains at the same temperature as the far field boundary of 15^{o}C.

The effect of the temperature variation upon the energy wall itself are likely to be significant, the thermal strains induced can cause significant variation in the bending moment and displacement of the wall and this will need to be closely monitored as the bending moment is already at the limits of its design envelope and significant variation could cause it to increase significantly. During the Winter Heating (Soil Cooling) Cycle there is a large temperature variation across the section of the wall which can cause variation in the change of thermal strains across the section which can lead to bending moment changes.

An important effect of the thermal expansion arises not from the variation in thermal strains but the gross change in thermal strains, which is the vertical displacement of the entire wall, this can have significant effects on the above surface parts of the station box.

The excess pore pressures generated by the thermal cycles are expected to be quite small, thus the permeability that the model was generated with was deemed acceptable for the purposes of consolidation, the majority of consolidation of the small variation was deemed to have occurred during the six month cycles.

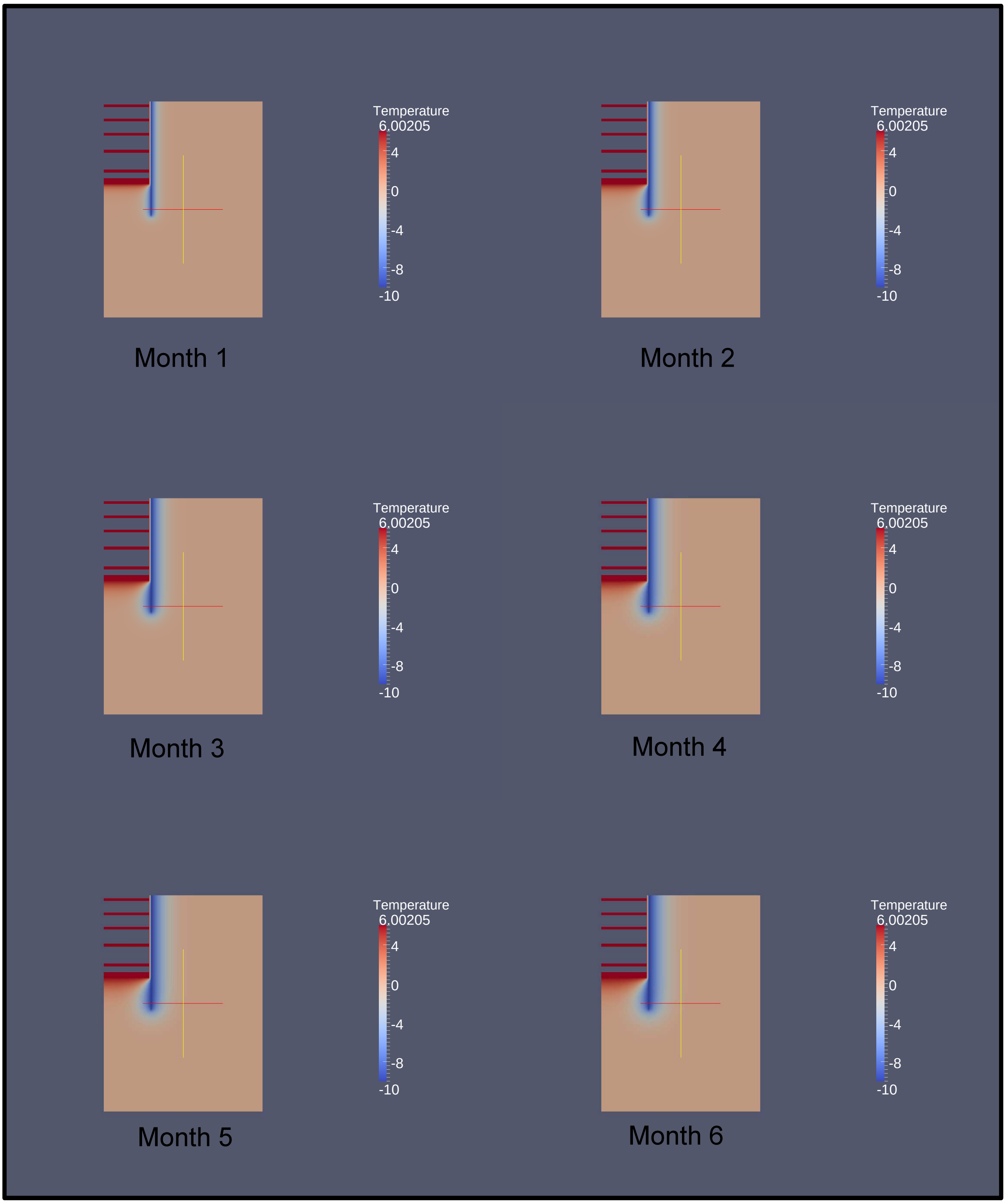

Figure 3.2.1 Temperature Variation During Winter Heating (Soil Cooling Cycle) (+12°C due to model)

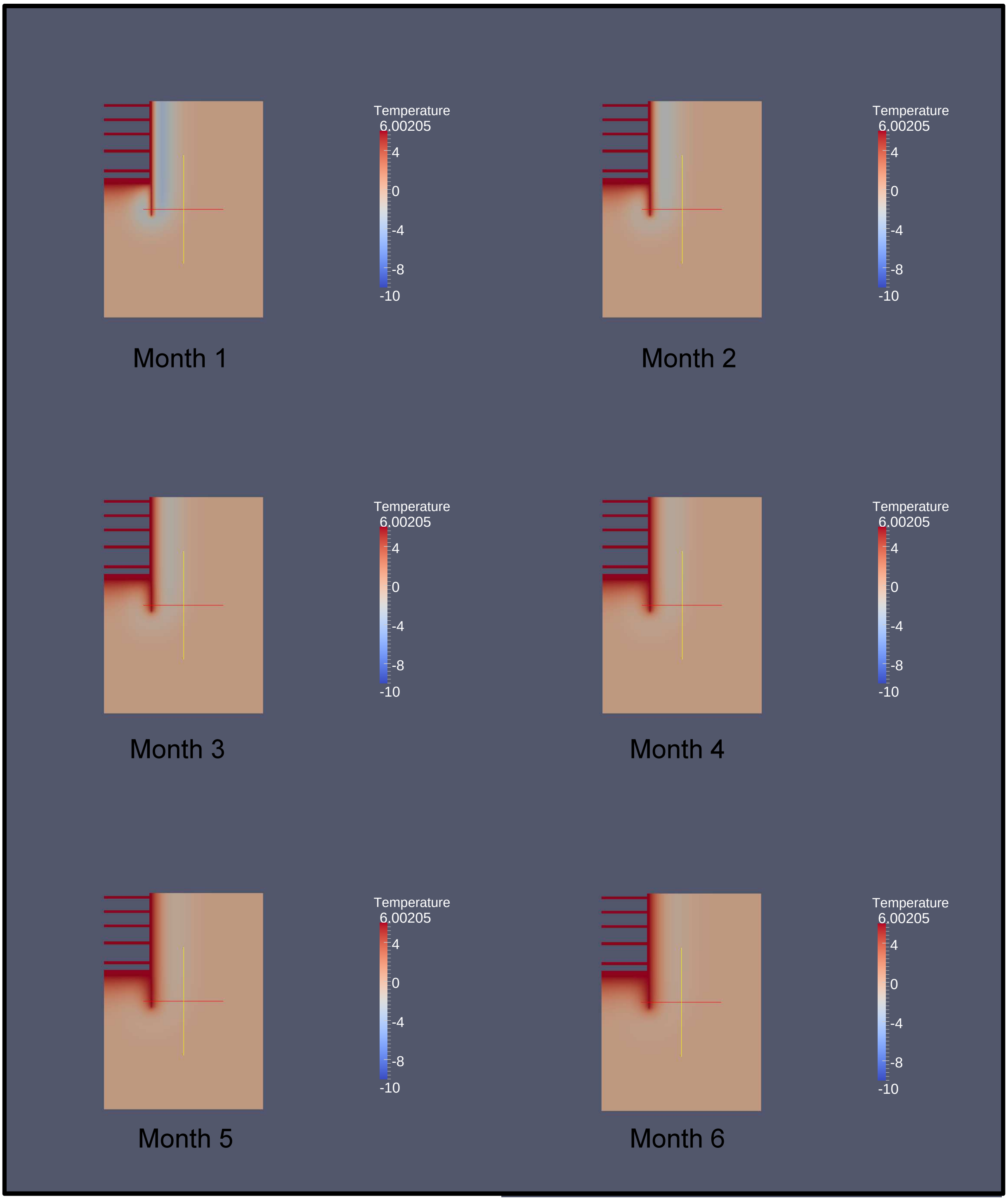

Figure 3.2.2 Temperature Variation During Summer Recharge(Soil Heating Cycle) (+12°C due to model)

Horizontal Displacements

The horizontal displacements induced by the heating and recharge cycles were not significant. Figure 3.2.3 shows the variation in wall displacement at the most critical region identified during the construction sequence, at 104mATD the midpoint between Prop 4 and the Base Slab.

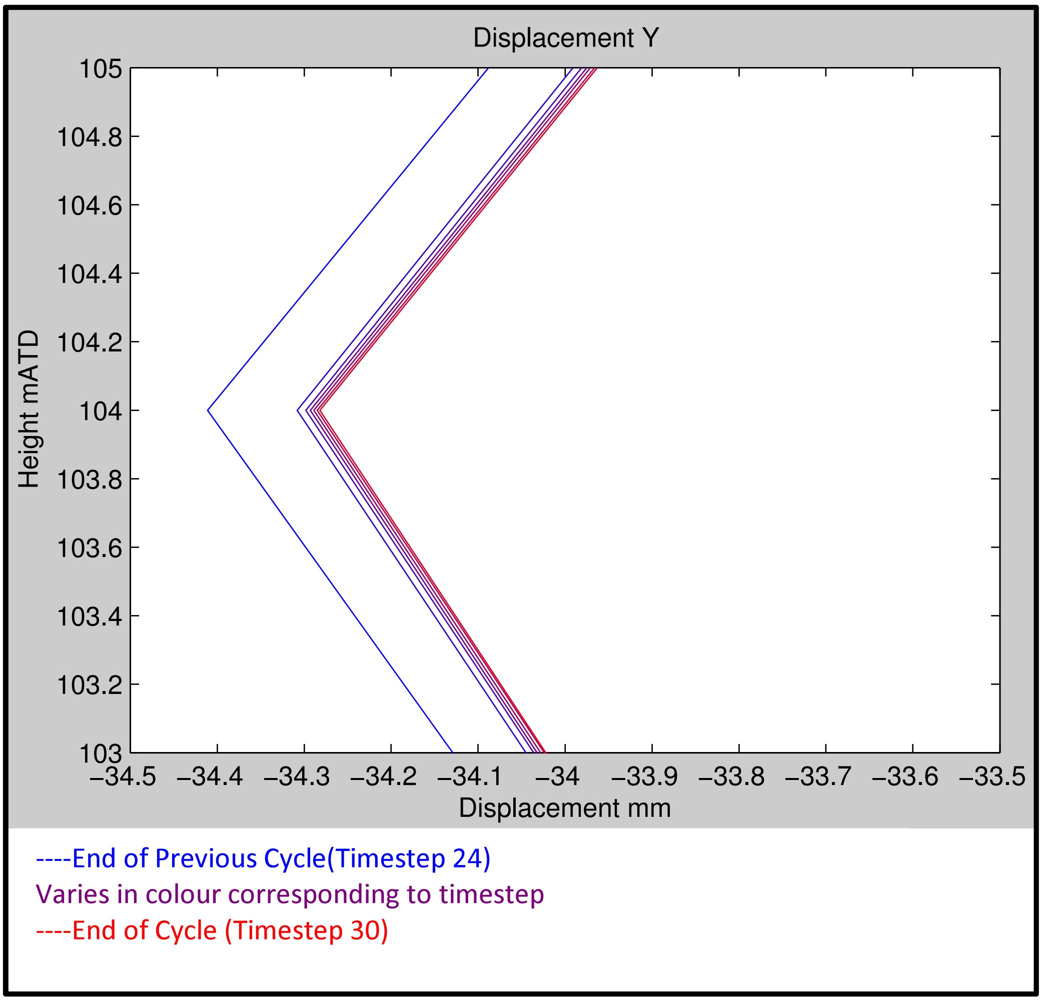

Figure 3.2.3 Displacements of the wall at most critical point during Winter Heating (Soil Cooling)

The change in displacement is the greatest during the first month and then slowly reduces, this change in displacement is purely due to consolidation from the negative excess pore pressures set up as no excavation was occurring. As the negative pore pressures dissipate pore fluid flows from the unexcavated soil and causes the wall to relax back as the effective stress acting on the wall decreases to compensate for the change in pore pressure. This process begins with the largest rate because the excess pore pressures are greatest, as they dissipate the excess pore pressure is lower thus the rate of consolidation becomes lower and the change in displacement becomes lower, the bunching up of the displacement lines at the end of the cycle in Figure 3.2.3 reflect this. The total change in displacement can be seen from the figure to be from -34.4mm to -34.3mm, a total reduction in displacement of 0.1mm, this is 0.3% of the total displacement set up from the construction sequence.

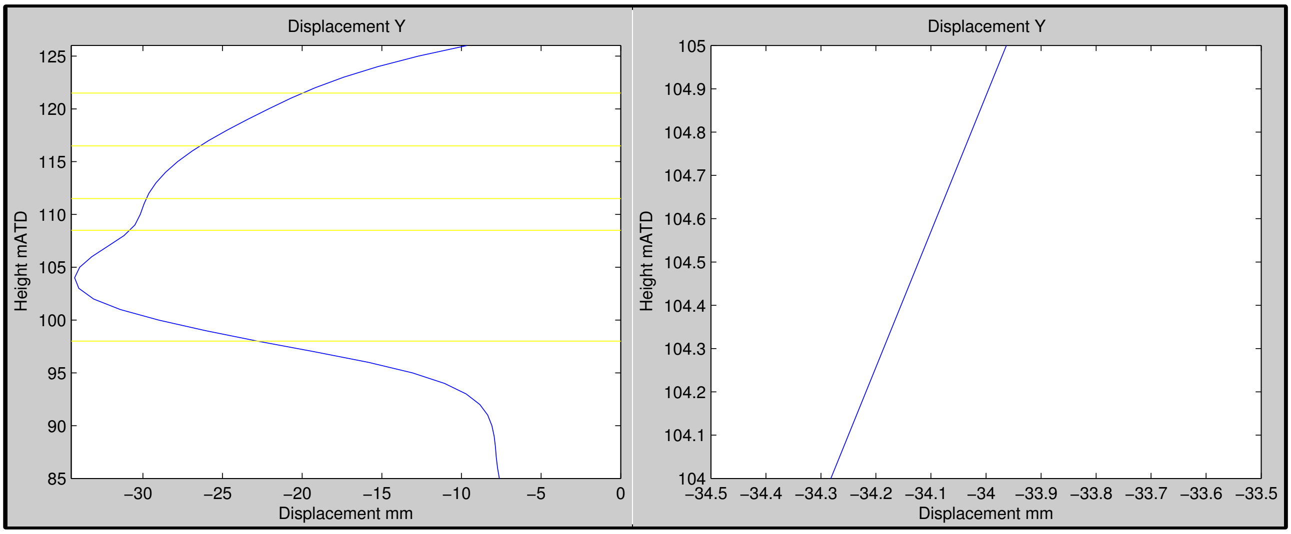

Figure 3.2.4 Displacements at the outset of the Summer Cycle for 20 years of operation

The effect of seasonal operation of energy wall upon the displacement is of extreme importance, if hysteresis is present then the relatively small displacements from one Winter cycle can cause significant displacements in the long term. Figure 3.2.5 shows that this is not the case however. The figure shows the displacements at the beginning of the cooling cycle for every Winter cooling cycle over a 20 year period and there is no modelled variation suggesting there is no hysteresis. This is likely due to the relatively small excess pore pressures arising from the thermal variation allowing consolidation to happen very quickly. This is likely also to be coupled with the equalising effect of the Summer operation which effectively balances the displacement caused by the Winter operation.

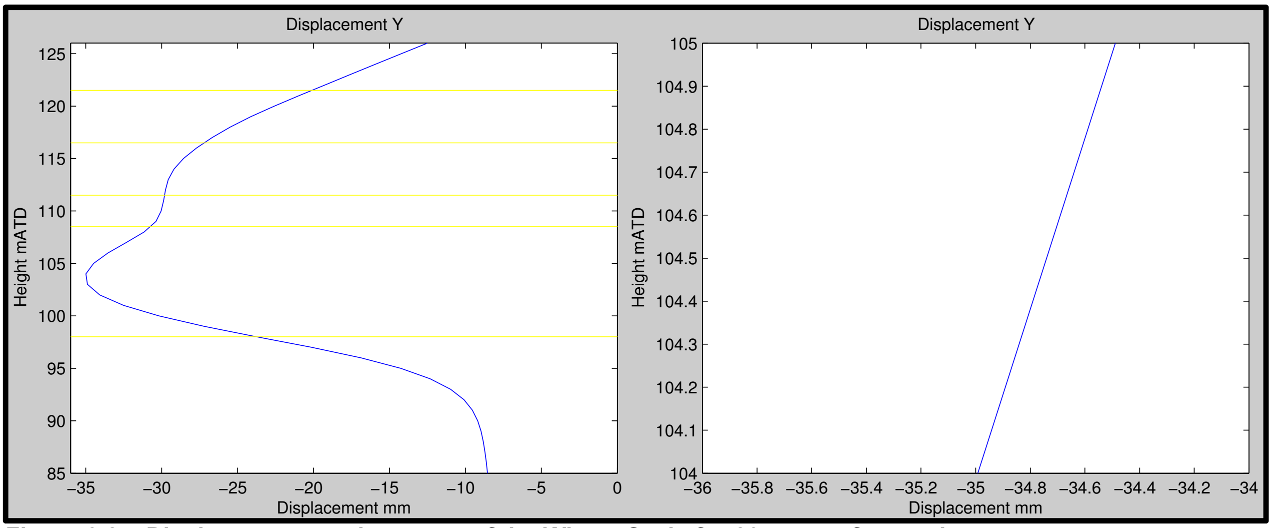

Figure 3.2.5 Displacements at the outset of the Winter Cycle for 20 years of operation

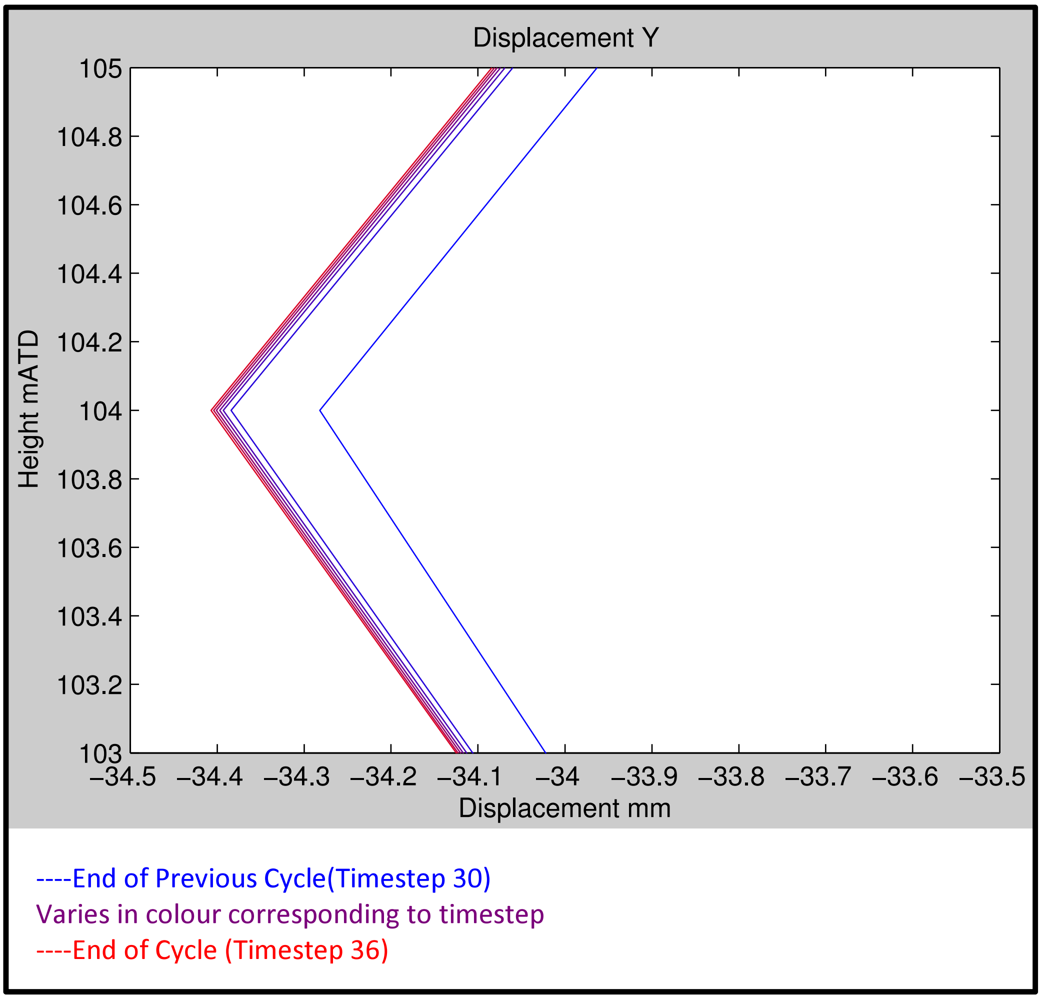

Figure 3.2.6 Displacements of the wall at most critical point during Summer Recharge (Soil Heating)

From the result in Figure 3.2.5 it is expected that similar behaviour will occur during the Summer Recharge (Soil Heating) cycle. Figure 3.2.4 and Figure 3.2.6 show that the behaviour is the same and that the displacements mirror those from the Winter Cycle; the change in displacement in the first month is the largest and then the changes reduce as time progresses due to the variations in excess pore pressure described earlier for the Winter Cycle, the difference being that we would expect a positive pore pressure to develop during the Summer Cycle, the movement of the Pore Fluid over time would increase the effective stresses on the wall causing displacement into the station. The displacement from the Summer Cycle was from -34.3mm to -34.4mm a total change 0.1mm which was the direct opposite of the Winter Cycle of 0.3% of the total displacement.

Figure 3.2.4 can be seen to tie up the other end of Figure 3.2.5 showing that throughout successive cycles there is no hysteresis in the Summer Cycle either, throughout twenty years of seasonal operation the initial displacement at the beginning of the Summer Cycle is the same each time.

3.2.2 Vertical Displacement

Vertical Displacement at the head of the wall has significant effects upon the structure above the station box. Figure 3.2.7 shows the variation in vertical wall

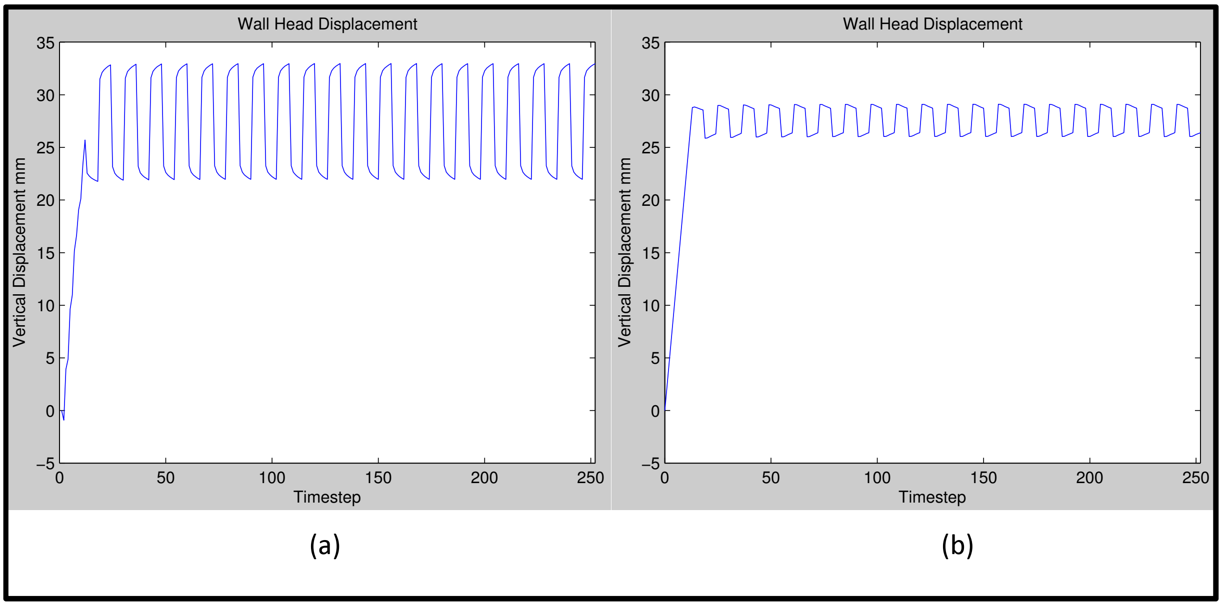

Figure 3.2.7 Vertical wall (a)head and (b)toe displacements for 20 years of operation

displacement from the initial construction all the way through 20 years of seasonal operation at the wall head (a) and the toe (b). The maximum variation during the seasonal cycling is 10mm increase during the Summer recharge (soil heating) and a 10mm decrease during the Winter heating. In the same way that the wall displaces into the soil during a Winter cycle the wall also displaces downwards due to the reduction in effective stress and vice versa during a Summer cycle. In the same way that it was shown there was no hysteresis on the horizontal displacements it was also ascertained that there was no hysteresis from the seasonal operation here.

From Figure 3.2.7 it can be seen that there is also movement of the base in the opposite direction showing that thermal expansion and contraction occur in both directions in the wall. The vertical movement at the head of the wall is greater in magnitude during the seasonal operation than the movement at the base; this shows that there is also bulk movement of the wall during the seasonal operation as well as the thermal expansion and contraction.

The model is limited that it only models the vertical wall displacements at the middle of the wall on one side of the station, thus further research must be done to ascertain differential settlements caused by the perpendicular wall and by corner effects.

3.2.3 Pore Pressure

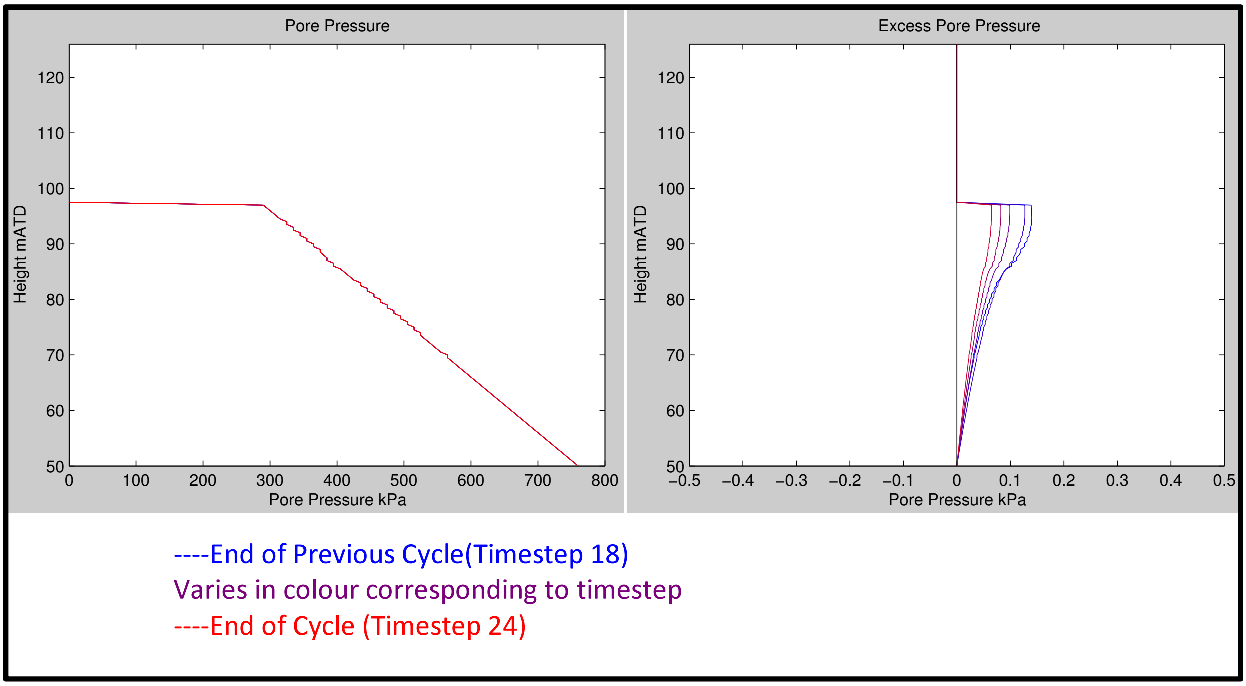

Figure 3.2.8 Pore Pressure and Excess Pore Pressure Summer Recharge (Soil Heating)

The excess pore pressures developed during the seasonal operation of the energy wall are incredibly small compared to those that are developed during the construction sequence. Figure 3.2.7 and Figure 3.2.9 show the development of the excess pore pressure on the stations side of the wall with -0.13kPa developing at the outset of the Winter cycle and only 0.13kPa at the beginning of the Summer Cycle. As has been previously discussed the consolidation during the six months causes the magnitude of the pore pressures to reduce over time as the pore fluids flow in to alleviate negative excess pore pressure or flow out to alleviate positive excess pore pressure.

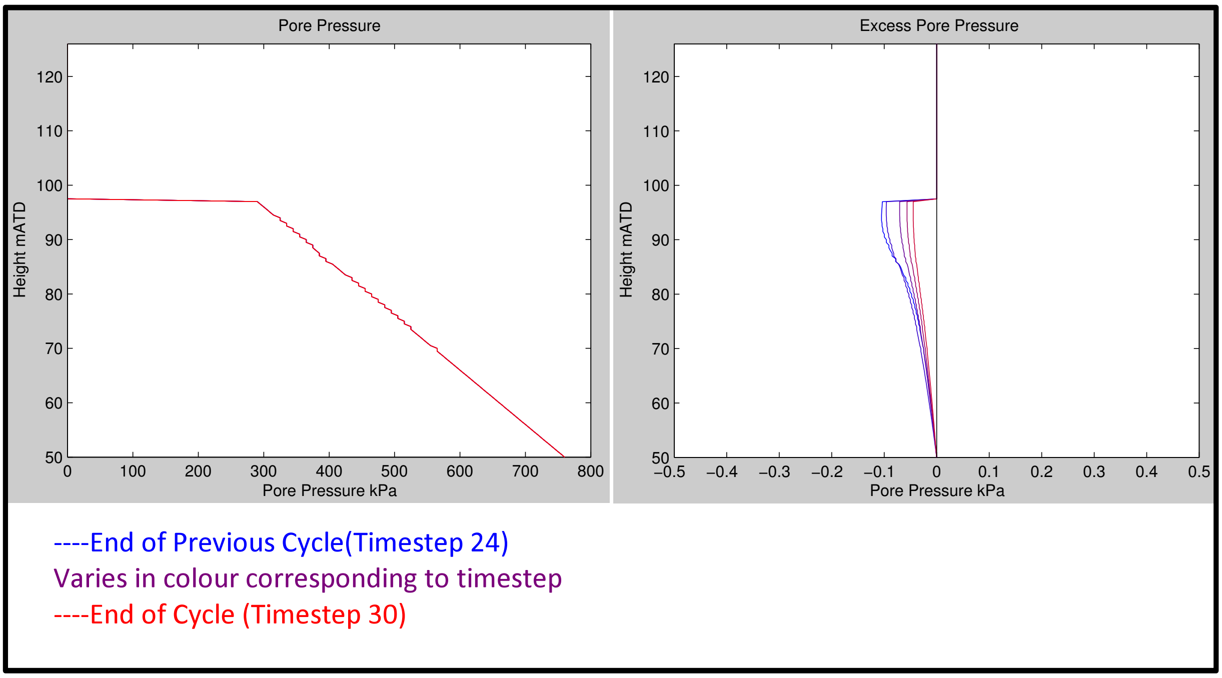

Figure 3.2.9 Pore Pressure and Excess Pore Pressure Winter Heating (Soil Cooling)

Compared to the excess pore pressures developed during construction which had a maximum of -35kPa in Figure 3.1.7(b). Figure 3.2.10 shows that the same effect occurs on the unexcavated side of the soil.

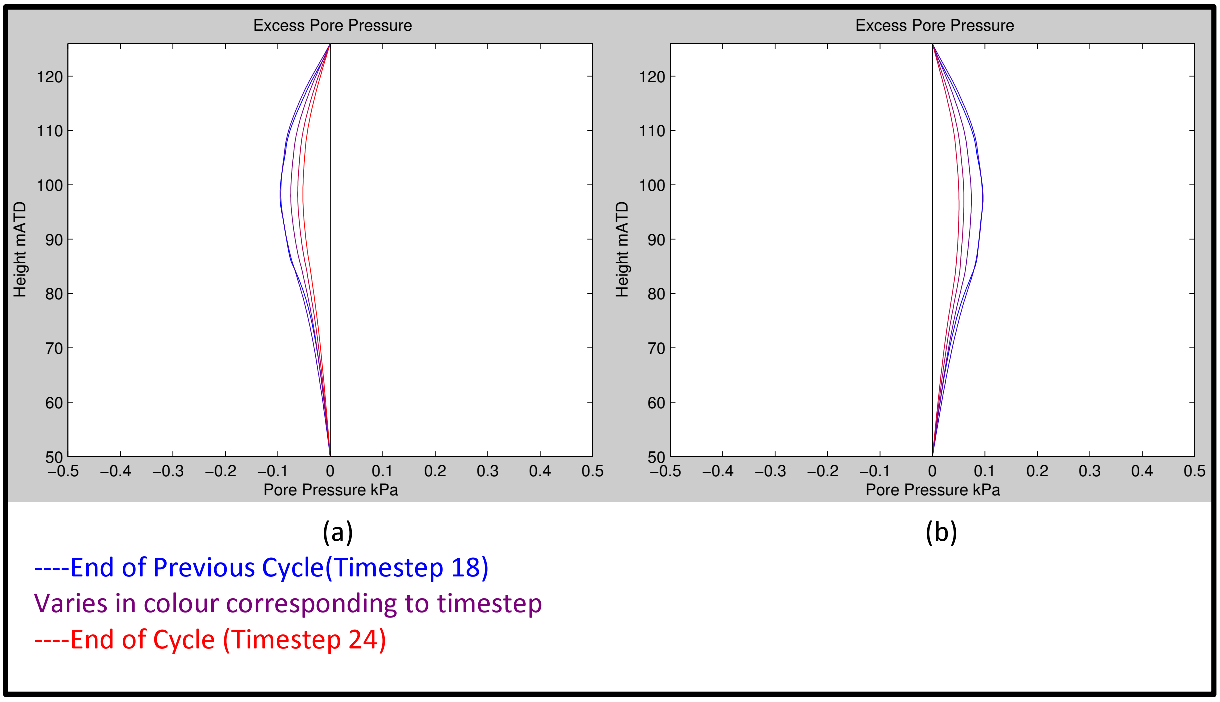

Figure 3.2.10 Excess Pore Pressure for Winter(a) and Summer(b) cycles on Unexcavated Side

As was mentioned earlier it is important to establish the cumulative hysteresis effect that the seasonal operation has on the pore pressure of the soil as this has consequences on the effective and total pressures and therefore the bending moments induced in the wall. Figure 3.2.11 shows the excess pore pressures on the unexcavated side of the wall developed at the outset of both the Winter and Summer cycles over the modelled operating life of 20 years and just like before there is cumulative effect seen as all the plots are the same with each timestep. The same behaviour was true for the station side.

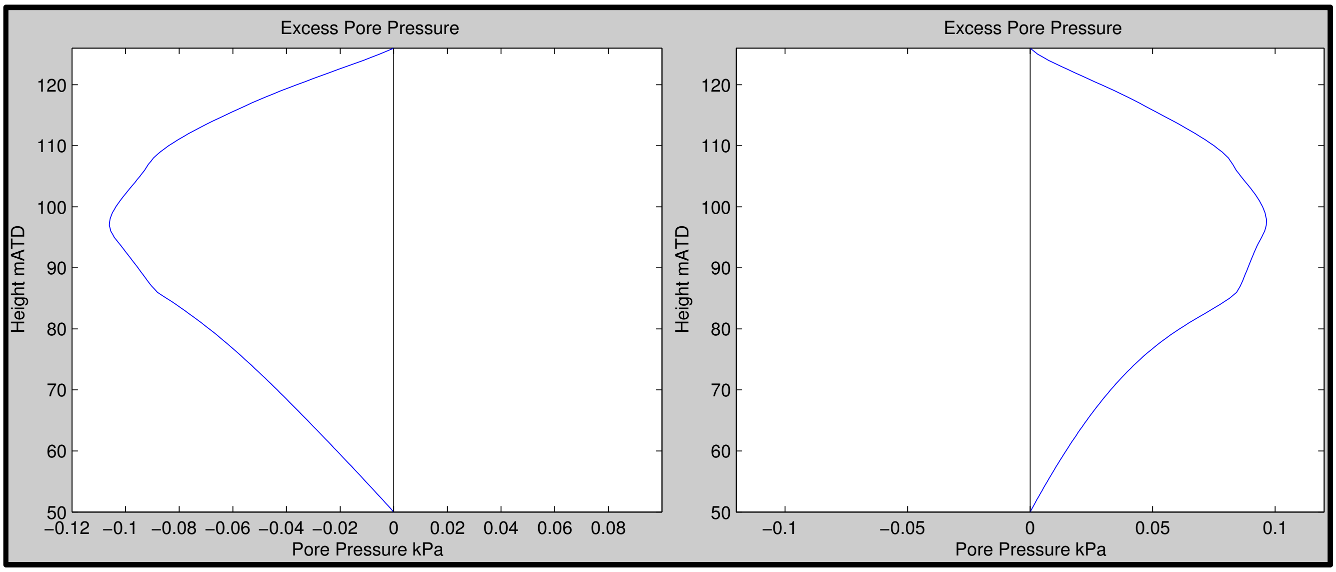

Figure 3.2.11 Excess Pore Pressure at the outset of Winter(a) and Summer(b) cycles over 20 years (Unexcavated)

3.2.4 Excess and Total Stress

The seasonal operation of the energy wall has an effect upon the effective and total stresses developed in the soil. During a Winter cooling cycle as shown in Figure 3.2.12 the cooling effect on the soil causes thermal contraction of the pore fluid

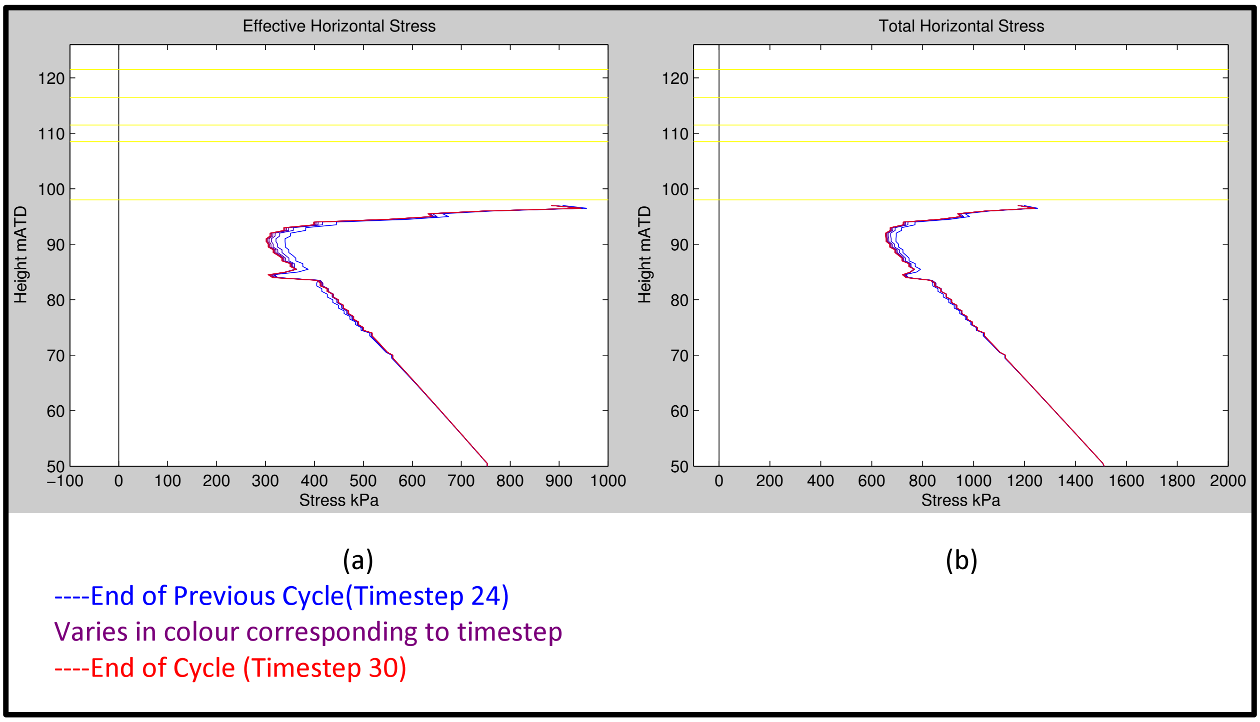

Figure 3.2.12 Effective (a) and Total (b) Stress on Station Side of Wall during a Winter Cycle

same variation on the effective stress as well. During the Summer recharge soil heating cycle the pore fluid and soil structure undergo thermal expansion which causes the total stress and effective stress to increase throughout the cycle and mirror the changes that arise from the Winter cycle.

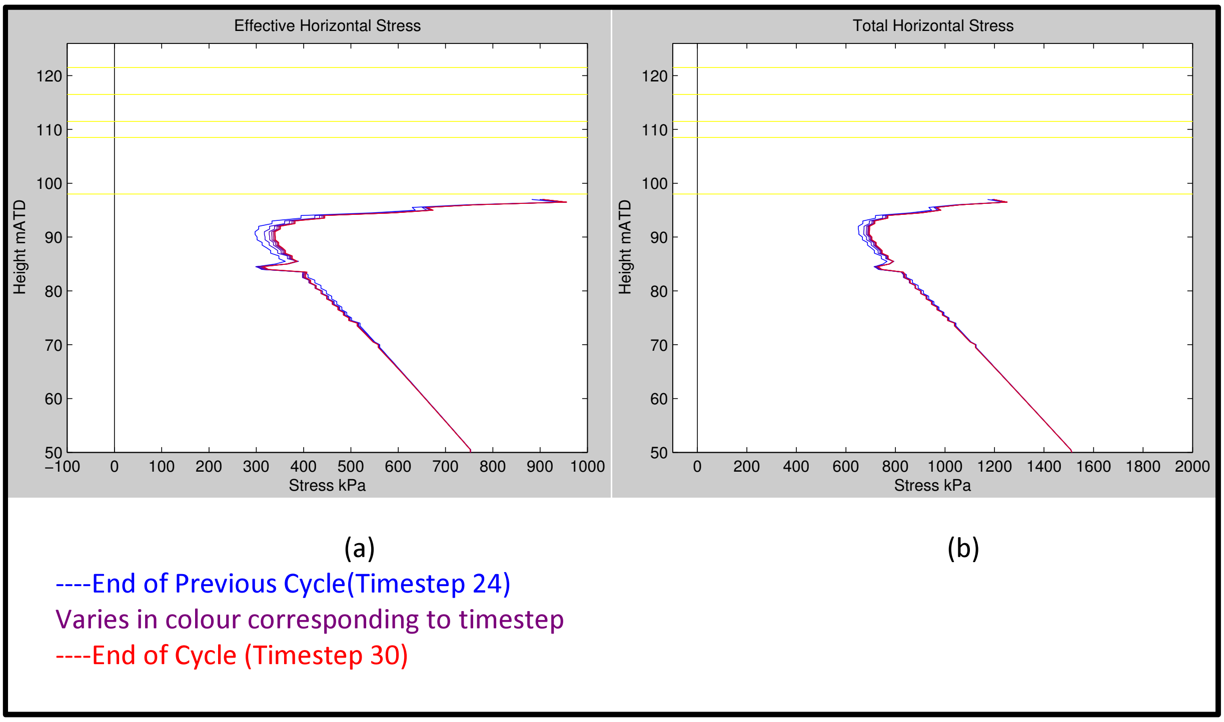

Figure 3.2.13 Effective (a) and Total (b) Stress on Station Side of Wall during Summer Cycle

Figure 3.2.13 shows the effective and total stress variation through during a Summer Recharge cycle. The variation throughout the twelve months is only 50kPa reduction during a Winter cycle and a 50kPa addition during the Summer cycle at the top of the excavation from the beginning to the end of a cycle.

Similarly to previous sections there are no cumulative effects from the seasonal operation on the effective or total stress. Figure 3.2.14 shows the horizontal effective stress at the outset of both Summer and Winter cycles plotted over 20 years of operation and just like the pore pressure and displacements no hysteresis occurs between cycles. This was the same result for total stress for both Station Side and the Unexcavated Side of the wall for both Horizontal and Vertical stresses.

The effective and total stresses acting on the unexcavated side of the wall varied in

the same way as on the station side, decreasing during a Winter soil cooling cycle and increasing in a Summer recharge cycle. This can be seen in Figure 3.2.15.

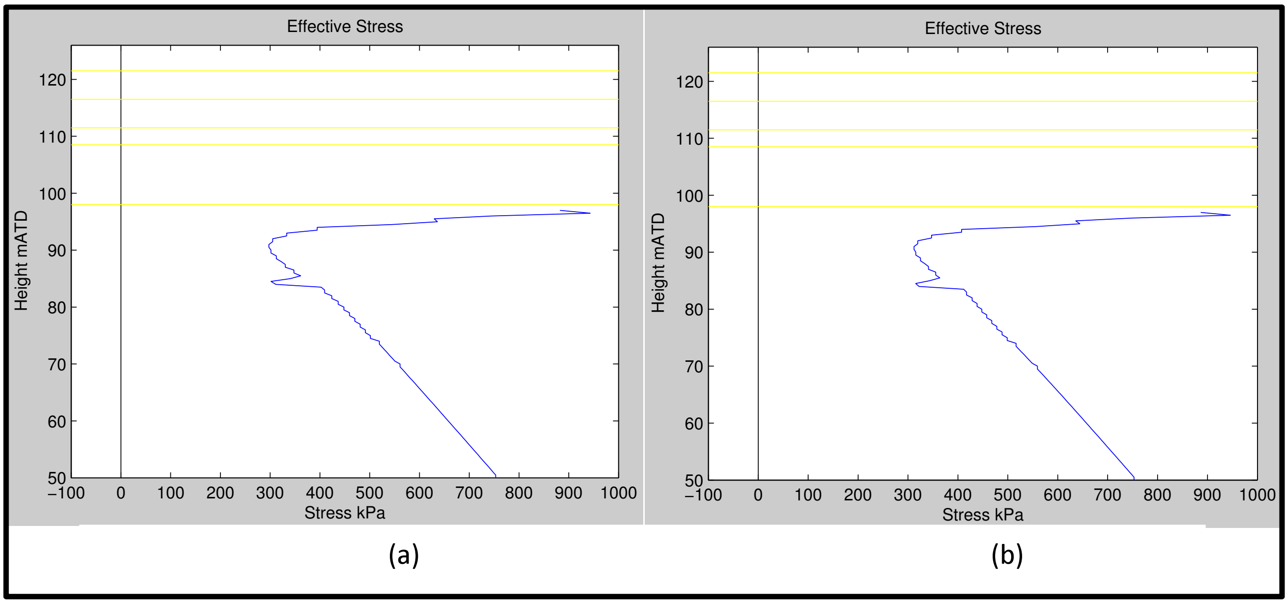

Figure 3.2.14 Effective Horizontal Stress Variation throughout 20 years of operation at the outset of (a)Summer and (b)Winter Cycle

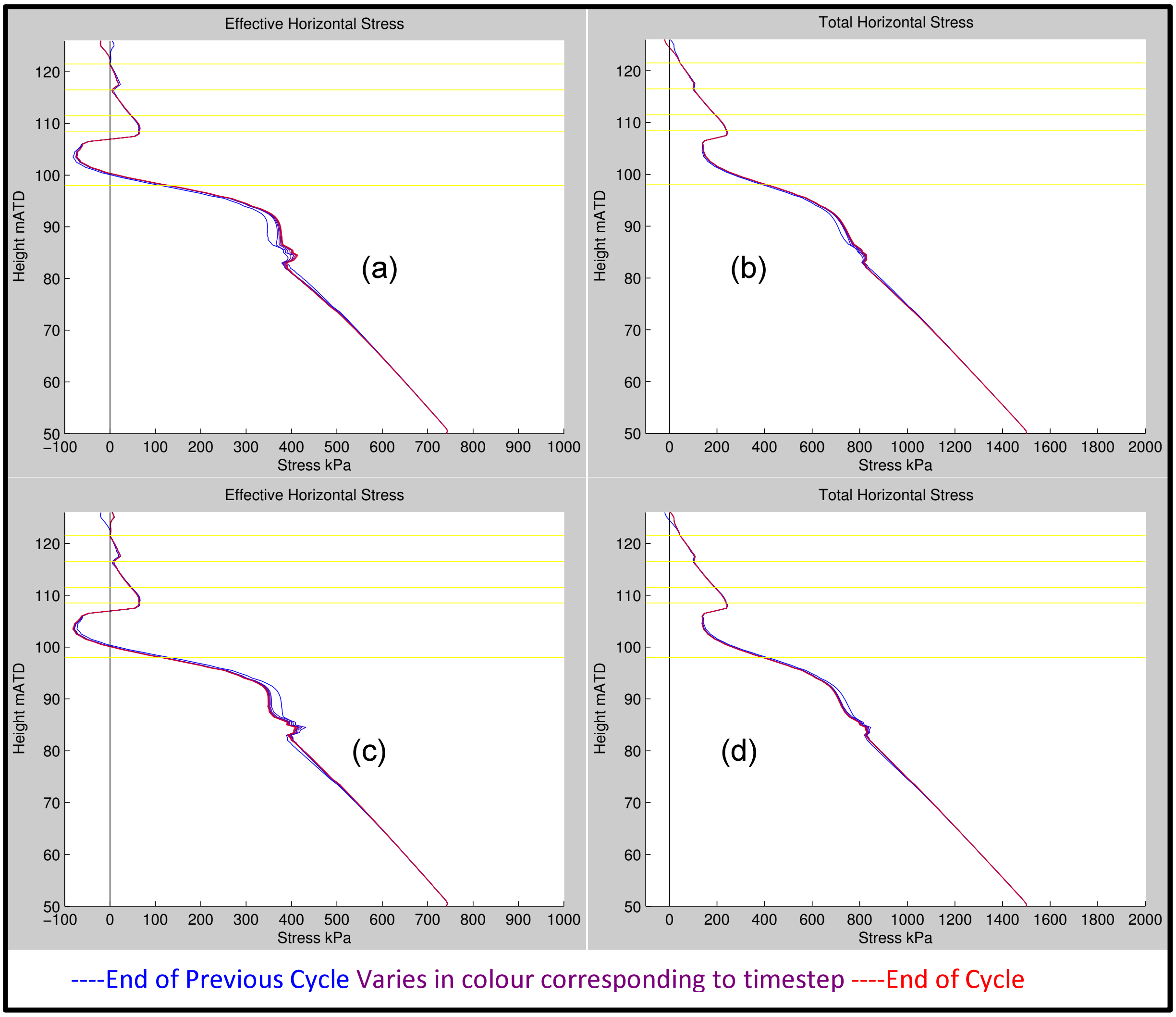

Figure 3.2.15 Effective and Total Horizontal Stress during Summer (a) and (b) and Winter (c) and (d) Cycles on Unexcavated Face of the Wall

3.2.5 Bending Moment

The variation of bending moment with the seasonal operation of energy wall is not only the most important aspect of this study, due to how close the modelled construction sequence was to the bending moment envelopes in Figure 3.1.10, it also varies quite significantly between the Winter and Summer Cycles.

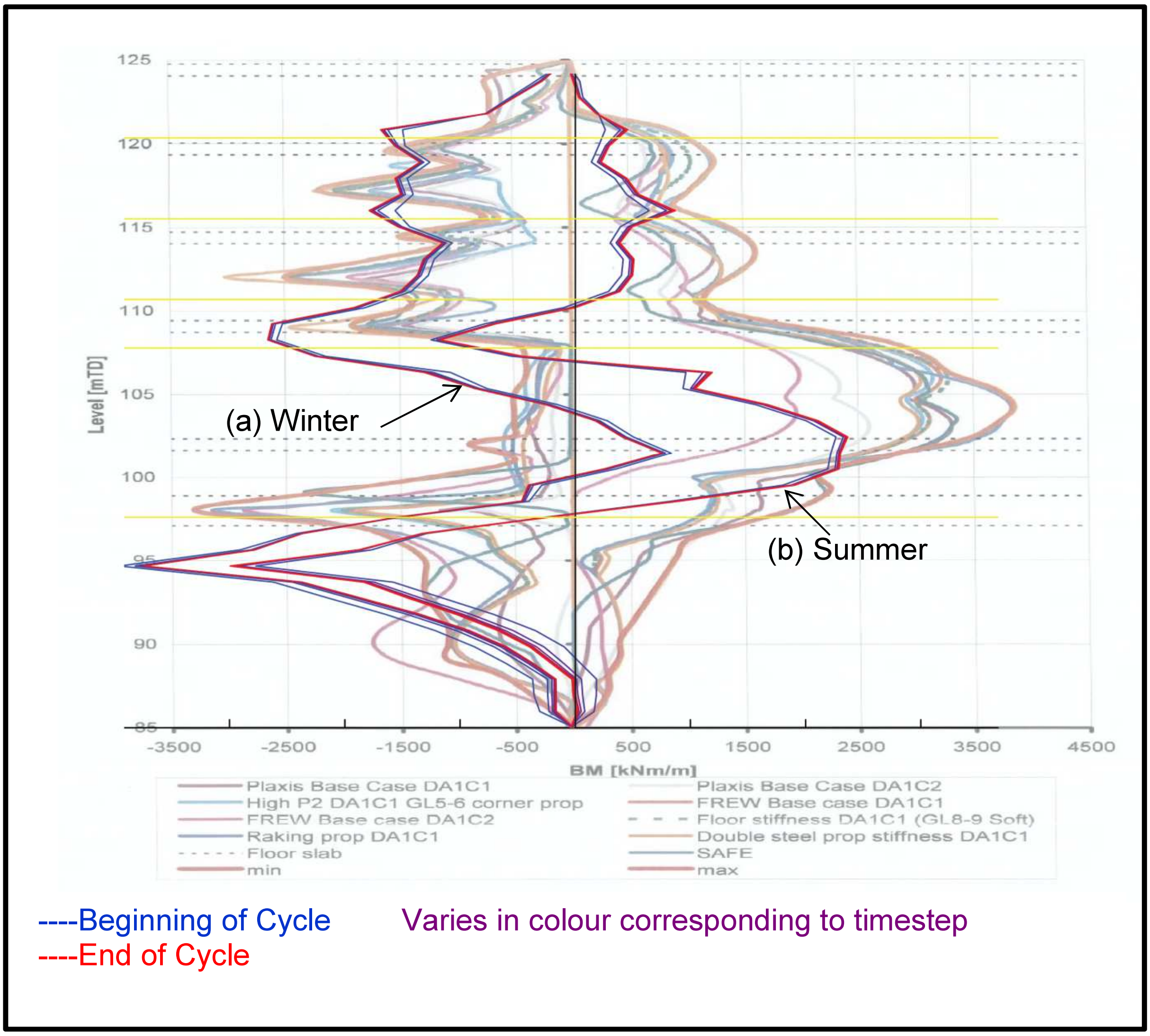

Figure 3.2.16 Bending Moment From (a)Winter (b)Summer Cycle with Arup envelopes

Figure 3.2.16 shows how large the variation is from the end of each cycle to the outset of the next operating cycle. The difference in the first 30 day cycle is -1.4MNm/m from the end of the Summer Cycle to the beginning of the Winter Cycle and 1.4MNm/m at the end of the Winter Cycle to the beginning of the Summer Cycle at the fourth slab level. This is quite a large change, about 35% of the maximum bending moment (at 95mATD) and is problematic as the bending moment is far beyond Arup's design bending moment envelopes. The large change is due to the thermal strains that develop during Winter Cycle, the conditions show that the station is constantly held at 18^{o}C and during the Winter Operation the primary GSHP circuit in the energy wall contains fluid held at 2^{o}C. This causes a temperature gradient of 16^{o}C across the section of the energy wall causing large thermal strains to develop. The direction of these thermal expansions causes the wall to bulge into the station which is restricted by the slabs. This causes an increase in reaction force and therefore bending moments due to the slabs.

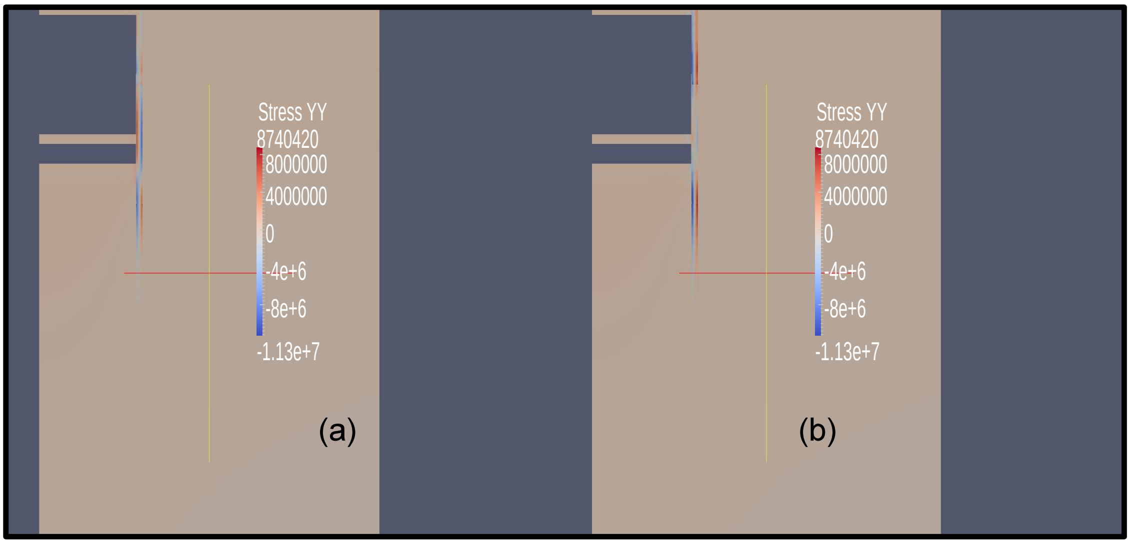

Figure 3.2.17 Vertical Stress Variation in the Wall from the end of the (a) Summer Cycle to the beginning of (b) Winter Cycle (Pascals)

Figure 3.2.17 shows the variation in YY Stress throughout the wall, the variation through the section of the wall which governs the bending moment. The stresses across the section of the wall at the base slab level becomes increases quite a lot between the two cycles as explained above.

As with the other properties that vary with the seasonal operation the Bending Moment does not exhibit any cumulative effects over the twenty years of seasonal operation of the energy wall, seen by a plot over the twenty years of the operation in Figure 3.2.18. This is to be expected from the previous results as vertical effective stresses which govern the bending moment also doesn't have a cumulative effects.

3.2.6 Surface Settlement

The settlement of the soil beyond the wall increases (displaces downwards) by 10mm throughout a Winter Cycle and reduces by 10mm (displaces upwards) by 10mm during a Summer Cycle as seen in Figure 3.2.19. This matches up with the

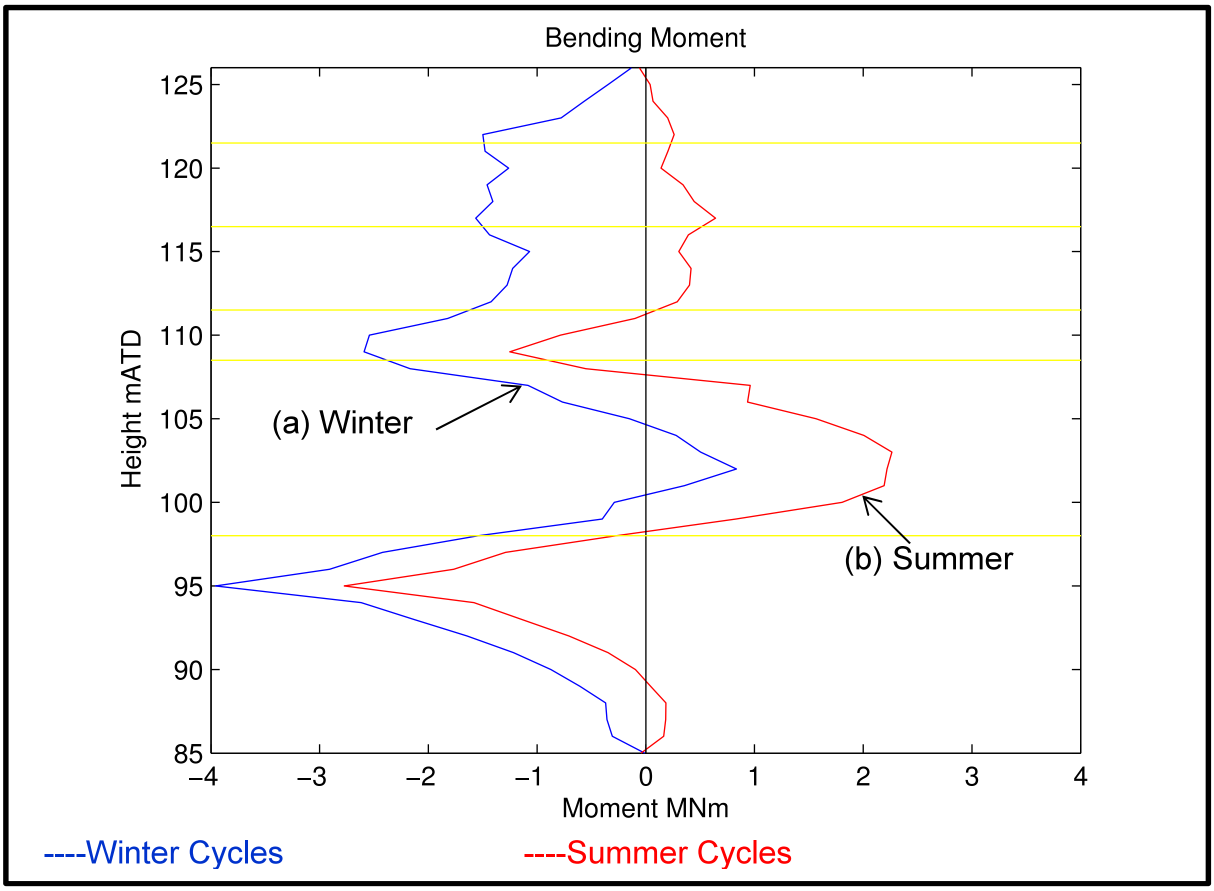

Figure 3.2.18 Bending Moment of (a) Winter and (b) Summer Cycles over 20 years of operation.

vertical displacements of the head of the wall which exhibits the same vertical displacements as seen in Figure 3.2.7.

During a Winter Cycle the soil is cooled which causes thermal contraction of the pore water and the soil structure which causes the settlement to increase, this is change is greater closer to the wall as the temperature change is greatest closer to the wall and changes most at the beginning of each cycle as the temperature change is greatest at the beginning as seen in Figure 3.2.1 and Figure 3.2.2.

In the same way as with the other effects of the seasonal operation of the energy wall have no cumulative effect upon the surface settlement of the soil beyond the wall. This is evidenced in Figure 3.2.20 which also allows the 10mm displacement characterised earlier to be seen very easily. As has been mentioned earlier the grout compensation has the effect to stiffen the soil against surface settlement, therefore

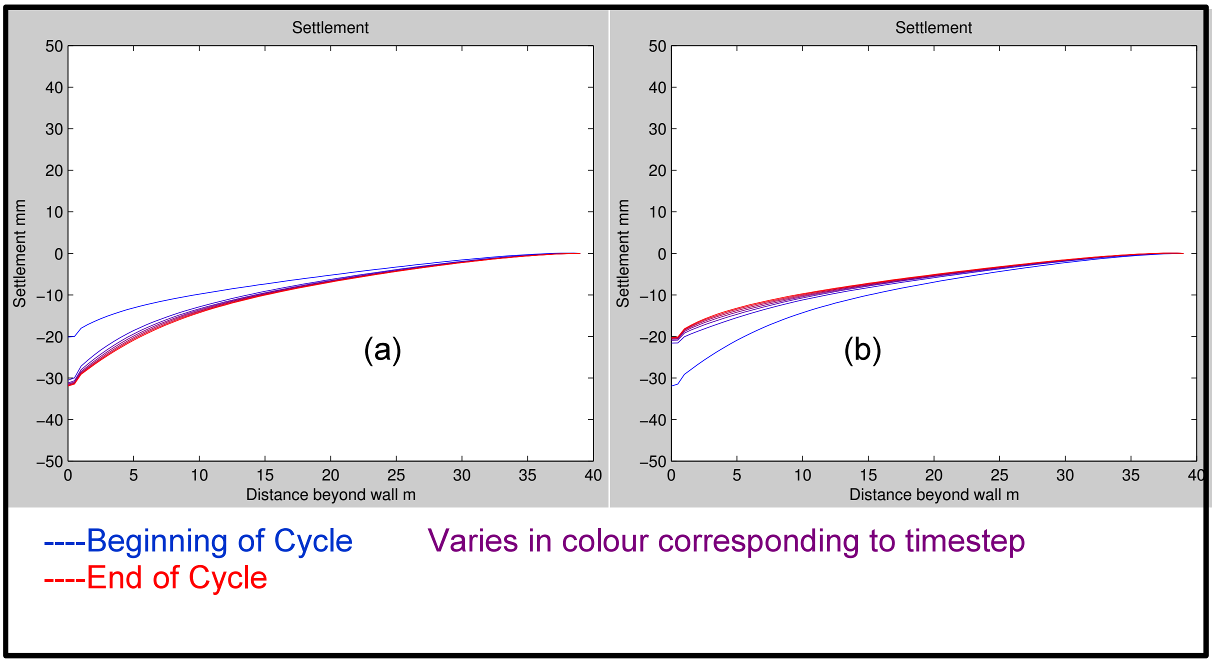

Figure 3.2.19 Settlement Profile of the Ground Beyond the Wall during (a) Winter and (b) Summer Cycles

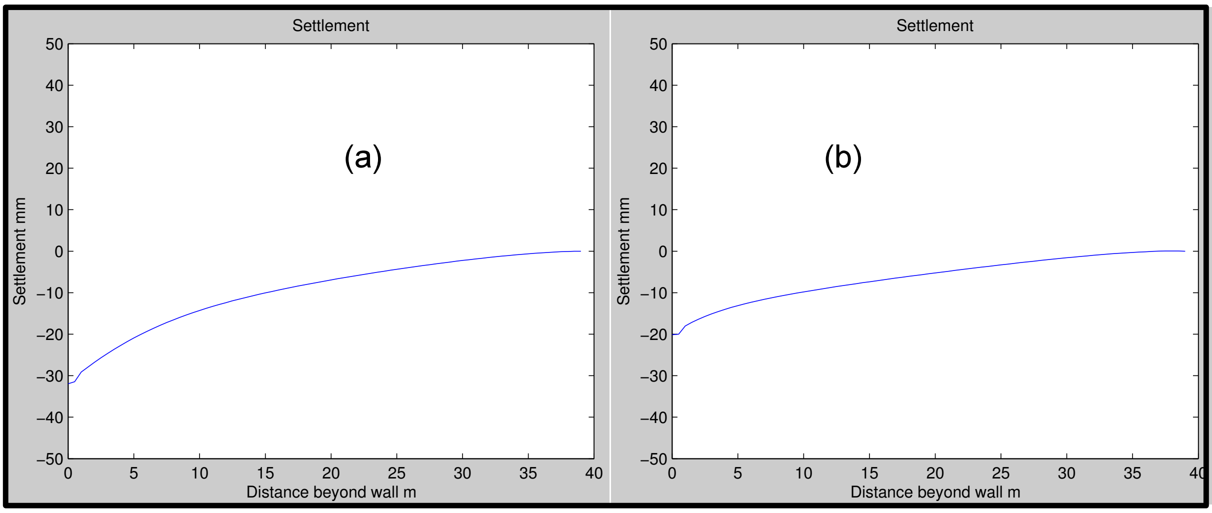

Figure 3.2.20 Settlement Profile of the Ground Beyond the wall at the beginning of (a) Winter and (b) Summer of a 20 year operation

the change in soil stiffness is likely to reduce the soil settlement, however further study would have to be conducted to determine the true effects as no surface settlement data was given in order to calibrate the surface settlement. The effect upon the serviceability limit state of the surrounding buildings due to the seasonal operation of the energy wall is beyond the scope of this study and further research would be required to determine the effects.

4.0 Conclusions

From the THM analysis of the energy wall the seasonal operation appears to have no cumulative effect upon the geotechnical properties of the soil and the structural properties of the energy wall in the 20 year seasonal operation modelled. Assuming this result is true it is possible to look at the effects of seasonal operation in any cycle as a characteristic result for any cycle throughout the twenty year cycle. Further research comparing in situ data of actual energy foundations throughout an extended operating cycle with modelled data would be required to validate this result.

The pore pressure, effective stress, total stress and horizontal wall displacement changes are so small they are not significant compared to that of the original construction sequence. The bending moment variation is relatively large due to the temperature gradient through the section of the wall during a Winter Cycle. The Summer Cycle is essentially soil recharge so the bending moment profile is almost the same as that of the construction sequence, the Winter Cycle however increases the maximum bending moment from -3MNm/m to -4MNm/m. This result moves the bending moment profile far beyond the safe Arup envelope; although this is still within the M_P bounds of 7.5MNm/m, this is still beyond the safe operating conditions the designers had designed for and is of concern to the designers. As the bending moment envelope that was provided did not account for the omission of the fifth prop it is likely that the design envelopes are slightly larger, however as this has not been provided this is of concern to the designers who should use this data as feedback into their operational design. As such further research with in situ data from site would be required to validate the results from a computational model based approach to the seasonal operation of energy foundation results.

5.0 Suggestions for Further Work

- Revise the model to follow the actual construction stages including cutting the heave piles at each level.
- After a number of years of operation of the energy wall conduct research to compare the actual operating displacements and stresses with those that were modelled in order to validate the results presented in this report, especially the lack of cumulative effect upon all geotechnical properties and the rate of pore pressure dissipation.
- Use a more advanced Mohr-Coulomb model in the openFTL/geoKit to prevent the possibility of negative effective stresses that arose in Figure 3.1.9.
- Obtain revised design bending moment envelopes from the designers in order to compare the bending moment with envelopes that omit the fifth prop in the station.
- Perform more advanced analysis on the seasonal operation of the GSHP including modelling the effects of daily usage to take into account more detailed fluctuations in the bending moment at the beginning of both the Winter Cycle and the Summer Cycle.
- Revise the model to look at other sections within the station box including sections with tunnels and the effects at the intersection of the tunnel and wall.
- Perform more detailed calibration to compare the surface settlement with settlement profiles obtained on site in order to better determine the effect of the seasonal operation of the GSHP on the surrounding structures in the highly urbanised area around Dean Street.

6.0 Appendix

Risk Assessment Retrospective

The initial project risk assessment analysed the risks of working in an office environment. The workplace that I was assigned moved through the duration of the project onto a lower table which did not have an office chair, as such the risk assessment was insufficient to have been able to model the effects of this change. Fortunately it transpired that remote access of the computer was available and therefore I was able to work in the environment of my own desk which has a monitor that could be raised and an operator chair. In retrospect there were a number of risks which should have been analysed more thoroughly, the risk of injury through RSI should have been highlighted as higher during periods of intense typing which would have led to work being spread out over a longer period of time. Eye strain, bad posture, lack of ventilation and hydration lead to performance impacts which could have been alleviated had they been highlighted earlier, the correct evaluation of this is related to the progress and success of the project.

The site visit I had organised was done outside of the project time constraints and a separate risk assessment was carried out for this, in retrospect it would have been wise to include the possibility of further site visits, although no other site visits took place.

Project Programme

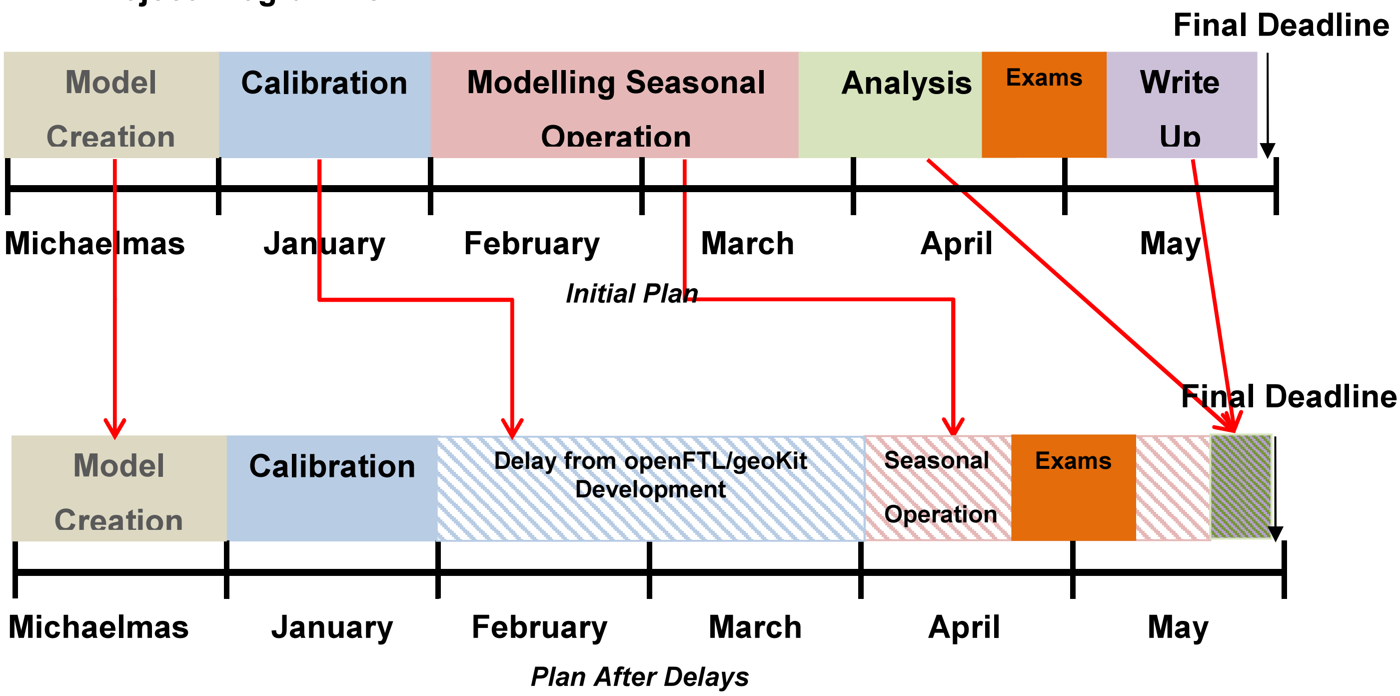

7.0 References

[1] T. Amis, "Energy Foundations in the UK," Geothermal International Ltd, 2011.

[2] H. Brandl, "Energy foundations and other thermo-active ground structures," *Geotechnique,* vol. 56, no. 2, pp. 81-122, 2006.

[3] B. A. K. S. T. A. C. &. P. P. P.J. Bourne-Webb, "Energy Pile Test at Lambeth College, London: Geotechnical and Thermodynamic Aspects of Pile Response to Heat Cycles," *Géotechnique,* vol. 59, no. 3, pp. 237-248, 2009.

[4] Y. Rui, "Finite Element Modeling of Geothermal Problems - First Year Report," 2011.

[5] B. S. L. R. R. C. G. H. J. Lund, "Geothermal (Ground-Source) Heat Pumps," *Renewable Energy World,* vol. 6, no. 4, July-August 2003.

[6] FWT Ltd., "Seasonal Ground temperature," [Online]. Available: http://www.filterclean.co.uk/closed_loop_heat_pumps.asp. [Accessed 25 05 2013].

[7] "Thermal Pile Design, Installation & Material Standards," Ground Source Heat Pump Association, 2012.

[8] D. Garber, " Implementation and Validation of Ground Source Heat Pump System Models in an Integrated Building and Ground Energy Simulation Environment - First Year Report," 2011.

[9] M. N. a. L. V. Lyesse Laloui, "Experimental and numerical investigations of the behaviour of a heat exchanger pile," *International Journal of Numerical and Analytical Methods in Geomechanics,* no. 30, pp. 763-781, 2006.

[10] R. Rawlings, "Ground Source Heat Pumps - A Technological Review," *A BSRIA Technical Note,* 1999.

[11] A. D. D. &. C. Davidson, "Ground Source Heat Pump System. Design Statement. TOttenham Court Road, Dean Street," Geothermal International & Crossrail, 2011.

[12] Cementation Skanska, "Knightsbridge Palace Hotel," Cementation Skanska, 2012.

[13] A. P. D. H. &. R. M. L. Wong, "Analysis Report for 3D FE Model of Tottenham Court Station West Box"," Crossrail Design Consultant Framework Contact C122 - Bored Tunnels, 2011.

[14] D. Nicholson, "Assessing the latest advances in thermal piling," Piling and Foundations UK, Arup, 2011.